Northumbria Research Link

Impact of Channel Correlation on Different Performance Metrics of OSSK-Based FSO System

Richa Priyadarshani, *Student Member, IEEE*, Anshul Jaiswal, *Member, IEEE*, Manav R. Bhatnagar, *Senior Member, IEEE*, Jan Bohata, Stanislav Zvanovec, *Member, IEEE*, and Zabih Ghassemlooy, *Senior Member, IEEE*

Abstract—In this paper, we study the impact of correlation on the bit error rate (BER) and the channel capacity of a free-space optical (FSO) multiple-input-multiple-output (MIMO) system employing optical space shift keying (OSSK) over a fading channel. In order to study a practical correlated channel, we consider the effect of channel correlation due to both small-and large-scale eddies and show that the use of OSSK over correlated FSO channel can lead to an improved system performance with increasing correlation level of upto 0.9. In this work, we first develop an analytical framework for different performance metrics of the OSSK multiple-input single-output system with correlation and then extend our investigation by proposing an asymptotically accurate mathematical framework for MIMO. We also validate all the analytical results using MATLAB simulations. Finally, we develop an experimental setup of FSO with two correlated links to study the throughput and latency of the links at different turbulence levels.

Index Terms—Arbitrary correlation, bit error rate, discrete-input continuous-output (DCMC) capacity, free-space optical (FSO) communications, Gamma-Gamma ($\Gamma\Gamma$) distribution, Green's matrix, MIMO, optical space shift keying

I. INTRODUCTION

Recently, spatial modulation (SM) has been proposed as a novel and promising technique for radio-frequency (RF) communications, which offers improved spectral efficiency (SE) and performance at reduced data-processing complexity, compared with other widely adopted multiple-input-multiple-output (MIMO) schemes [2]–[4]. SM exploits both signal and spatial-constellations for data transfer by encoding a unique sequence of bits for intensity modulation of a single transmitter (Tx)-laser, while the remaining Txs are in the off-state. In [5], optical SM (OSM) was proposed, which provided a simple solution in free-space optical (FSO)-MIMO systems with reduced inter-channel interference (ICI), simpler decoding, and improved inter-antenna synchronization (IAS). Space shift keying (SSK)– a special case of SM for an RF channel and introduced in [6]–[8]–exploits only the spatial positions of Txs to encode the information bits thereby trading off the receiver's complexity against the data rate. A similar concept was adopted in [9], to develop the doppelganger of SSK for FSO with atmospheric turbulence (AT), termed as optical SSK (OSSK).

OSSK is a simplified version of OSM benefiting from its advantages such as reduced ICI, simpler decoding, etc., and has motivated researchers to investigate for indoor and outdoor environments. In [10], [11], analyses and practical implementations of these schemes in indoor scenarios (i.e., static channel with no randomness) were reported. However, in outdoor applications with AT, which is caused due to inhomogeneities in the temperature and pressure of the atmosphere with time, evaluation of various performance metrics for OSM/OSSK becomes a tedious task [12], [13]. In [12], it was shown that OSM offers an improved performance than conventional optical modulation methods in terms of power and SE with reduced decoding complexity. In [9], the bit error rate (BER) performances of OSSK under saturated and weak AT regimes are evaluated using negative exponential and lognormal models, respectively.

In [9]–[14], it was assumed that the channel is uncorrelated, which is not true for practical outdoor FSO-MIMO links with closely spaced multiple apertures. The spatial correlation among different channel gains can be caused due to various reasons such as close proximity of optical Txs and receivers (Rxs), antenna arrangement, angle spread, and angle of arrival (AOA), etc. However, for the line of sight (LOS) path between the Txs and the Rxs, angle spread and AOA are usually not considered as the dominant reasons for spatial correlation. Therefore, the effect of correlated channels due to insufficient antenna spacing on different performance metrics of a FSO system must be considered for a more realistic study [15]. There exist few works on OSM/OSSK under the correlated indoor environment [16]–[18]. In [16], OSM was shown to be more robust to high channel correlation compared with other multi-antenna schemes, however, AT was not considered in this work. In addition, the performance of SM/SSK considering correlated RF channels were investigated in [19] and [20]. But to the best of authors knowledge, no literature is available on the performance of OSM/OSSK under correlated outdoor FSO-MIMO channels. Therefore, the evaluation of different performance metrics of OSSK/OSM under correlated AT channels is still an important open research problem. In this paper, for the first time, the BER performance and the achievable capacity of an OSSK based FSO-MIMO system over an AT induced correlated channel are investigated. The reason for considering OSSK over OSM in this work is

A part of this paper was presented at the IEEE International Symposium on Communication Systems, Networks, and Digital Signal Processing (CSNDSP)-2018, Budapest, Hungary, July 18-20, 2018 [1].

R. Priyadarshani and M. R. Bhatnagar are with the Department of Electrical Engineering, Indian Institute of Technology Delhi, New Delhi 110016, India (e-mails: richa.priyadarshani, manav@ee.iitd.ac.in).

A. Jaiswal is with the Department of Electronics and Communication Engineering, Indian Institute of Technology Roorkee, 247667, India (e-mail: anshjasifec@iitr.ac.in).

Jan Bohata S. Zvanovec are with the Department of Electromagnetic Field, Faculty of Electrical Engineering, Czech Technical University in Prague, 16627 Prague, Czech Republic (e-mail: bohatja2, xzvanove@fel.cvut.cz).

Z. Ghassemlooy is with the Optical Communications Research Group, School of Computing, Engineering and Information Sciences, Northumbria University, Newcastle upon Tyne, NE1 8ST, U.K. (e-mail: z.ghassemlooy@northumbria.ac.uk).

because of the fact that OSSK is a special case of OSM with the dominant error in OSM (an error in the detection of the Tx's index - see Type-IV error in [12]) is the only error in OSSK. Therefore, the conclusions drawn from this work can also be used to infer the behavior of OSM over the correlated outdoor environment. In the above-rendered context, we outline the following novel contributions claimed in this paper:

- A generalized statistical analysis is performed to derive the joint probability density function (pdf) expression of arbitrarily correlated gamma-gamma ($\Gamma\Gamma$) random variables (RVs) by considering correlation among small-and-large-scale eddies (SLSE). Note that, the derived pdf can be easily mapped to the uncorrelated pdf and also to the scenario where only large-scale eddies are correlated.
- Using the joint pdf of the correlated $\Gamma\Gamma$ RVs, we derive a novel analytical expression for the pdf of the difference of arbitrarily correlated RVs. The resulting expression is used to derive *average pair-wise error probability (APEP), average BER (ABER), and channel capacity (b/s/Hz)* of OSSK over correlated FSO-MIMO.
- In order to extricate some *useful insights on coding gain (G_c) and diversity order (G_d) of the proposed system*, we perform asymptotic BER analysis at high signal-to-noise ratio (SNR) levels.
- Finally, *we develop an experimental setup of the correlated FSO-MISO system* and studied the impact of AT and correlation on the throughput and latency of the link.

Note that, in our previous work on OSSK in [1], we considered only FSO-MISO with correlation because of large-scale eddies, which corresponds to a special case of the correlation model considered in the present work. Moreover, analytical results presented in [1] were limited only to ABER for MISO system as opposed to our current work, where we present both ABER and capacity of a OSSK MIMO followed by the experimental results. Also in [1], the asymptotic results discussing G_c and G_d were not considered.

II. PRELIMINARIES

A. System Model

Consider an $N_t \times N_r$ OSSK FSO-MIMO system, where N_t and N_r are the number of Tx-lasers and Rx-apertures, respectively. In OSSK, the encoder encodes $\log_2 N_t = m$ bits into the index of a single Tx by mapping each symbol into the spatial constellation vector $\mathbf{s} = [s_1, s_2, ..., s_{N_t}]^T$, where $\mathbf{s} \in \{i_1, i_2, ..., i_{N_t}\}$, with i_l being the lth column of the $N_t \times N_t$ identity matrix and $1 \le l \le N_t$ [6], [8]. A sequence of m-bits is transmitted using the index of the Tx, which is only active for data transmission while all other laser Txs are off. The transmitted optical signal from the active jth Tx propagates through the AT induced correlated fading channel and is collected by a photodetector using an optical lens at the Rx. The regenerated electrical signal vector $\mathbf{y} \in \mathbb{R}^{N_r \times 1}$ at the Rx is given as:

$$\mathbf{y} = \sqrt{E_b}\mathbf{H}\mathbf{s} + \mathbf{n}, \tag{1}$$

where the energy per bit $E_b = \frac{R^2 P_t^2}{N_r^2}$, P_t is the transmit power, and R is the photodetector responsivity, which is

considered 1 in this work [21, Fig. 2.21]. Further, $\mathbf{s}$ denotes an N_t dimensional vector as defined earlier, $\mathbf{n}$ represents an N_r dimensional noise vector (i.e., zero mean additive white Gaussian noise (AWGN)) with a power spectral density of $N_0/2$, and $\mathbf{H}$ is the $N_r \times N_t$ arbitrarily correlated channel gain matrix, containing the channel coefficients $h_{r,l}$, which denotes the correlated channel gain between the lth Tx-laser and the rth Rx-aperture specifying the channel gain coefficient with $1 \le r \le N_r$.

It is assumed that, a perfect channel state information is available at the Rx and the detector demaps the unique sequence of bits emitted by the encoder by estimating the active Tx-laser index. Accordingly, the Rx applies optimal detector as the maximum likelihood detector:

$$\begin{aligned} \hat{l} &= \arg\max_l f_Y(y|s_l, \mathbf{h}) \\ &= \arg\min_l \sum_{r=1}^{N_r} |y_r - RP_t h_{r,l}|^2, \end{aligned} \tag{2}$$

where $\hat{l}$ is the estimated Tx-laser index and $1 \le \hat{l} \le N_t$.

B. Channel Model

It is well established in literature that, the $\Gamma\Gamma$ AT model provides an excellent match between the theoretical and experimental data for weak-moderate-strong AT [21]–[23]. Therefore, in this paper, we will model the channel fading $h_{r,l}$ using the correlated $\Gamma\Gamma$ distribution. Note that, we consider the outdoor downlink wireless channel model from the base station (BS) to the subscriber unit (SU). It is assumed that, antennas at the SU are sufficiently spaced and the correlated fading channel exists due to the closely spaced Txs at the BS [24]. Therefore, for the rest part of the paper we will drop the subscript r from $h_{r,l}$ for simple notations. In case of $\Gamma\Gamma$ model, the received irradiance h_l is considered to be the product of two gamma RVs, x_l and y_l, which denote the irradiance fluctuation contributions due to large- and small-scale eddies, respectively. The pdf of $\Gamma\Gamma$ Rv ($h_l = x_l y_l$) with no correlation can be expressed as [21], [23]:

$$f_{H_l}(h_l) = \frac{2(\alpha\beta)^{\frac{(\alpha+\beta)}{2}} h_l^{(\frac{(\alpha+\beta)}{2})-1}}{\Gamma(\alpha)\Gamma(\beta)} K_{\alpha-\beta}(2\sqrt{\alpha\beta h_l}), \tag{3}$$

where $K_v(\cdot)$ and $\Gamma(\cdot)$ are the modified Bessel function of the 2nd kind of order v [25] and the Gamma function, respectively, α and β are the AT parameters, which denote the effective numbers of large-scale and small-scale eddies, respectively with the effective sizes varying from the inner-scale to the outer-scale of turbulence denoted by l_0 and L_0, respectively. For a plane wave propagation with l_0 close to 0, i.e., a zero inner scale condition, α and β are given by [21], [23]:

$$\alpha = \left(\exp\left[\frac{0.49\sigma_R^2}{(1+1.11\sigma_R^{12/5})^{7/6}} \right] - 1 \right)^{-1}. \tag{4}$$

$$\beta = \left(\exp\left[\frac{0.51\sigma_R^2}{(1+0.69\sigma_R^{12/5})^{5/6}} \right] - 1 \right)^{-1}, \tag{5}$$

where σ_R^2 is Rytov variance, represents irradiance fluctuations due to AT, which is given by $\sigma_R^2 = 1.23C_n^2 k^{7/6} L^{11/6}$ and

$\sigma_R^2 = 0.5C_n^2 k^{7/6}L^{11/6}$ for the plane and spherical waves, respectively; C_n^2 is the refractive index structure parameter and $k = 2\pi/\lambda$ is the wavenumber [23].

In order to present a generalized and a practical model for the correlated AT channel, we consider moderate-to-strong AT by assuming both small-and-large-scale turbulent eddies contribute to the fading correlation. The correlation among the two gamma RVs x_i and x_j is defined by the correlation matrix $\mathbf{\Sigma}$ with elements of $\sigma_{i,j} \equiv 1$ for $i = j$ and $\sigma_{i,j} \equiv \rho_{i,j}$, $i \neq j$, with $i, j = 1, ..., N_t$. Note, $\sigma_{i,j} \in \mathbf{\Sigma}$. $\rho_{i,j}$ is defined as $\rho_{i,j} \triangleq \frac{\text{cov}(x_i, x_j)}{\sqrt{\text{var}(x_i)\text{var}(x_j)}}$, where $0 \leq \rho_{i,j} < 1$, $\text{cov}(\cdot)$ and $\text{var}(\cdot)$ denote the covariance and variance, respectively [26], [27], [28]. According to [29], the correlation coefficient $\rho_{i,j}$ also depends on the transversal distance between the apertures $d_{r_{i,j}}$ and the spatial coherence radius r_0, and for a given separation between the apertures, it can be obtained using:

$$\rho_{i,j} = \exp\left(-\left(d_{r_{i,j}}/r_0\right)^{5/3}\right). \quad (6)$$

Further, let us consider that, $\rho_{i,j}$ represents the effective correlation coefficient between the ith and the jth Txs, $\rho_{i,j}^{(\beta)}$ and $\rho_{i,j}^{(\alpha)}$ denote the correlation coefficients corresponding to the SLSE, respectively. Since, the large-and small-scale fading are considered to be independent of each other, for the identically-distributed and correlated $\Gamma\Gamma$ model, ρ can be given by [30]:

$$\rho_{i,j} = \frac{\alpha\rho_{i,j}^{(\beta)} + \beta\rho_{i,j}^{(\alpha)} + \rho_{i,j}^{(\alpha)}\rho_{i,j}^{(\beta)}}{\alpha + \beta + 1}. \quad (7)$$

It is evident from (7) that, for a given ρ there are an infinite number of possible solutions for $\rho_{i,j}^{(\alpha)}$ and $\rho_{i,j}^{(\beta)}$. Therefore, to generate the correlated $\Gamma\Gamma$ RVs, the challenge is to find the appropriate values of $\rho_{i,j}^{(\alpha)}$ and $\rho_{i,j}^{(\beta)}$ using (7) for the considered channel. Note, in [30, Section 5], the specific criteria for setting the large- and small-scale correlation coefficients based on the scintillation theory were proposed, which we can use to determine the parameters $\rho_{i,j}^{(\alpha)}$ and $\rho_{i,j}^{(\beta)}$. Following are the two most appropriate solutions valid for weak-moderate and moderate-strong AT:

- Scenario 1: The correlation among the large-scale edies is assumed to be dominant compared with the small-scale eddies, i.e., $\rho_{i,j}^{(\alpha)} < 1, \rho_{i,j}^{(\beta)} = 0$.
- Scenario 2: Both SLSE are equally contributing to the effective correlation, i.e., $\rho_{i,j}^{(\alpha)} = \rho_{i,j}^{(\beta)}$.

It is well established in literature that, for moderate AT, both Scenarios 1 and 2 are applicable, however, in case of strong AT only Scenario 1 is applicable [30].

Remark 1 (*Limitations of Scenario 1*): Since correlation among small-scale eddies is ignored in Scenario 1, the model is applicable for only lower values of ρ. E.g., for the minimum value of $\rho_{i,j}^{(\alpha)} = 0$ in (7) for moderate AT with $\alpha = 4, \beta = 1.9$, the solution of $\rho_{i,j}^{(\beta)} = 0$ will result in $\rho = 0$, while for the maximum value of $\rho_{i,j}^{(\alpha)} = 0.99$ in (7), we will have $\rho \approx 0.27$.

C. Statistics of the Correlated $\Gamma\Gamma$ AT Model

In order to study the system's behavior at high correlation values, the joint pdf applicable to Scenario 2 must also be derived. Therefore, by considering Scenario 2 in this section, we will derive a generalized joint pdf of the correlated $\Gamma\Gamma$ RVs, which will also be valid for both Scenario 1 and the uncorrelated system.

Consider $[x_1, ..., x_{N_t}]$ be a set of N_t correlated Gamma RVs with AT parameter α and correlation matrix $\mathbf{\Sigma}^{(\alpha)}$, which can be modelled using the following joint pdf expression [26], [28]:

$$f_{X_1,.....,X_{N_t}}(x_1, ..., x_{N_t}) = \frac{|\mathbf{W}^{(\alpha)}|^{\alpha}\exp(-\sum_{n=1}^{N_t}\frac{w_{n,n}^{(\alpha)}x_n}{\Omega^{(\alpha)}})}{\Gamma(\alpha)}$$

$$\times \sum_{i_1,...,i_{N_t-1}=0}^{\infty} x_1^{\alpha+i_1-1}x_{N_t}^{\alpha+i_{N_t-1}-1}(\Omega^{(\alpha)})^{-N_t\alpha-2\sum_{j=1}^{N_t-1}i_j}$$

$$\times \prod_{j=2}^{N_t-1} x_j^{\alpha+i_{j-1}+i_j-1} \prod_{n=1}^{N_t-1}\left[\frac{|w_{n,n+1}^{(\alpha)}|^{2i_n}}{i_n!\Gamma(\alpha+i_n)}\right], \quad (8)$$

where $|\cdot|$ denote the determinant and $\Omega^{(\alpha)} = E[x_i]/\alpha$. Further, $\mathbf{W}^{(\alpha)} = (\mathbf{\Sigma}^{(\alpha)})^{-1}$ and $w_{i,j}^{(\alpha)}$ denotes the elements of $\mathbf{W}^{(\alpha)}$. Note that, (8) is valid only for $\mathbf{W}^{(\alpha)}$ following the tridiagonal property. However, the inverse of $\mathbf{\Sigma}^{(\alpha)}$ is not always tridiagonal for all practical correlation models. Therefore, in this paper we will use Green's matrix approximation of $\mathbf{\Sigma}^{(\alpha)}$ and $\mathbf{\Sigma}^{(\beta)}$, respectively, in the analysis [28]. Similarly, the joint pdf of N_t correlated Gamma RVs, $[y_1, ..., y_{N_t}]$, with the AT parameter β and the correlation matrix $\mathbf{\Sigma}^{(\beta)}$ can be obtained by replacing α with β and $\mathbf{W}^{(\alpha)}$ with $\mathbf{W}^{(\beta)}$ in (8).

Then, a set of N_t correlated $\Gamma\Gamma$ RVs $[h_1, ..., h_{N_t}]$ can be generated as a product of two multivariate Gamma RVs $[x_1, ..., x_{N_t}]$ and $[y_1, ..., y_{N_t}]$, which arise from the large-and small-scale eddies, respectively [26], [30]; such that $h_i = x_i y_i$. Therefore, the joint pdf of the multivariate arbitrarily correlated $\Gamma\Gamma$-distributed RVs can be obtained using:

$$f_{H_1,..,H_{N_t}}(h_1,..,h_{N_t}) = \int_0^{\infty}\cdots\int_0^{\infty}\frac{f_{X_1,...,X_{N_t}}(x_1,..,x_{N_t})}{x_1 \cdot x_2 \cdots x_{N_t}}$$

$$\times f_{Y_1,..,Y_{N_t}}\left(\frac{h_1}{x_1},..,\frac{h_{N_t}}{x_{N_t}}\right)dx_1 \cdots dx_{N_t}. \quad (9)$$

By substituting (8) and $f_{Y_1,.....,Y_{N_t}}(y_1,....,y_{N_t})$ in (9) and employing [31, Eq. (3.471/9)], the joint pdf of correlated $\Gamma\Gamma$ RVs, with both SLSE contributing to the correlation, can be derived. Let us establish the following theorem based on the above-stated analysis:

Theorem 1: The joint pdf of arbitrarily correlated $\Gamma\Gamma$ RVs, by considering that correlation is stimulated due to both SLSE, is given by:

$$f_{H_1,...,H_{N_t}}(h_1,..,h_{N_t}) = \sum_{\substack{i_1,..,i_{N-1}=0 \\ t_1,..,t_{N-1}=0}}^{\infty} \varrho_{\alpha\beta} \prod_{j=1}^{N_t}\left[2h_j^{\beta+m_{\beta_j}-1}\right.$$

$$\times \left(\frac{w_{j,j}^{(\beta)}h_j\Omega^{(\alpha)}}{w_{j,j}^{(\alpha)}\Omega^{(\beta)}}\right)^{\frac{\alpha+m_{\alpha_j}-\beta-m_{\beta_j}}{2}}$$

$$\times K_{\alpha+m_{\alpha_j}-\beta-m_{\beta_j}}\left(2\sqrt{\frac{w_{j,j}^{(\alpha)}w_{j,j}^{(\beta)}h_j}{\Omega^{(\alpha)}\Omega^{(\beta)}}}\right)\right], \quad (10)$$

where $m_{\alpha_j} = i_j$ and $m_{\beta_j} = t_j$ for $j = 1$, $m_{\alpha_j} = i_{N_t - 1}$ and $m_{\beta_j} = t_{N_t - 1}$ for $j = N_t$, $m_{\alpha_j} = i_{j-1} + i_j$ and $m_{\beta_j} = t_{j-1} + t_j$ for $j = 2, 3, .., N_t - 1$, and

$$
\varrho_{\alpha\beta} = \frac{\Omega^{(\alpha)(-N_t\alpha - 2\sum_{j=1}^{N_t-1} i_j)} \Omega^{(\beta)(-N_t\beta - 2\sum_{j=1}^{N_t-1} t_j)}}{\Gamma(\alpha)\Gamma(\beta)}
$$
$$
\times |\mathbf{W}^{(\alpha)}|^{\alpha} |\mathbf{W}^{(\beta)}|^{\beta} \prod_{n=1}^{N_t-1} \left[\frac{|\, w_{n,n+1}^{(\alpha)}\, |^{2i_n}\, |\, w_{n,n+1}^{(\beta)}\, |^{2t_n}}{i_n! \Gamma(\alpha + i_n) t_n! \Gamma(\beta + t_n)} \right]. \quad (11)
$$

Note that, we have derived (10) by considering the correlation of Scenario 2, nevertheless, the derived expression is generalised and it can be easily mapped to the pdfs applicable to the correlation of Scenario 1 as well as the uncorrelated case. Later, we will discuss the mapping technique following the derivation of the ABER in Section III.

D. Instantaneous BER

We can use the widely accepted union bound technique to find a tight upper bound of BER for OSSK-FSO-MIMO in the form of [9]:

$$
\text{BER}_{\text{OSSK}}^{(u)} \leq \frac{1}{N_t \log_2(N_t)} \sum_{\substack{l_1=1 \\ l_2=1}}^{N_t} d_H(c_{l_1}, c_{l_2}) \text{P}(l_1 \rightarrow l_2), \quad (12)
$$

where $d_H(c_{l_1}, c_{l_2})$ is Hamming distance between the transmitted and received symbols c_{l_1} and c_{l_2}, respectively, by counting the number of bits in error. Note, for $c_{l_1} = c_{l_2}$, Hamming distance is zero. Moreover, $\text{P}(l_1 \rightarrow l_2)$ is the PEP between symbols c_{l_1} and c_{l_2}, which is given by:

$$
\text{P}(l_1 \rightarrow l_2) = Q\left(\frac{1}{N_r} \sqrt{ \frac{\bar{\gamma} \log_2 N_t}{2} \sum_{r=1}^{N_r} |\, h_{rl_1} - h_{rl_2}\, |^2 } \right), \quad (13)
$$

where $Q(\cdot)$ is Gaussian-Q function, $\bar{\gamma} = E_b T_b / (N_0 \log_2 N_t)$ is the average SNR and T_b is the symbol period. Note, h_{rl_1} and h_{rl_2} are the fading coefficients corresponding to the channel gain between the rth Rx and the l_1 and l_2 Txs, respectively, which are mathematically characterized as correlated $\Gamma\Gamma$ RVs.

E. Channel Capacity

There exists only a few works in literature, which have studied the capacity of the correlated FSO system. Most of the existing works have studied Shannon capacity of a FSO system, which is applicable to a continuous-input continuous-output memoryless channel. In such cases, the channel input is continuous-amplitude discrete-time defined by Gaussian distribution. E.g., the ergodic capacity of FSO-MIMO was studied in [32] by assuming a continuous input with Gaussian distribution. Nevertheless, in the case of a practical FSO-OSSK system, only a single laser is activated at a time. Therefore, it will be more pertinent to derive the discrete-input continuous-output (DCMC) capacity by considering the input alphabets to be finite instead of a Gaussian input and also the channel to be correlated. The DCMC capacity of a FSO system with OSSK is given as [33]:

$$
C_{\text{DCMC}} = \max_{f(\mathbf{x_1}),...,f(\mathbf{x_{N_t}})} \sum_{l=1}^{N_t} \int_0^{\infty} \cdots \int_0^{\infty} f(\mathbf{y} \mid \mathbf{x}_l) f(\mathbf{x}_l)
$$
$$
\times \log_2 \left(\frac{f(\mathbf{y} \mid \mathbf{x}_l)}{\sum_{m=1}^{N_t} f(\mathbf{y} \mid \mathbf{x}_m) f(\mathbf{x}_m)} \right) d\mathbf{y}, \quad (14)
$$

where $\mathbf{y}$ is the received signal vector (as given in (1)) and $\mathbf{x}_l$ is the signal vector transmitted over the channel, i.e., $\mathbf{x}_l = \sqrt{E_b} \mathbf{H} \mathbf{s}_l$. Note that, the capacity in (14) can be maximized for equally likely inputs, i.e., $f(\mathbf{x}_l) = 1/N_t$, which gives:

$$
C_{\text{DCMC}} = \sum_{l=1}^{N_t} \int_{N_r} \frac{1}{N_t} f(\mathbf{y} \mid \mathbf{x}_l) \log_2 \left(f(\mathbf{y} \mid \mathbf{x}_l) \right) d\mathbf{y}
$$
$$
- \sum_{l=1}^{N_t} \int_{N_r} \frac{1}{N_t} f(\mathbf{y} \mid \mathbf{x}_l) \log_2 \left(\sum_{m=1}^{N_t} \frac{1}{N_t} f(\mathbf{y} \mid \mathbf{x}_m) \right) d\mathbf{y}
$$
$$
= I_1 - I_2, \quad (15)
$$

where,

$$
f(\mathbf{y} \mid \mathbf{x}_l) = \frac{1}{(\sqrt{2\pi\sigma^2})^{N_r}} \exp\left(- \sum_{r=1}^{N_r} \frac{(y_r - x_{rl})^2}{2\sigma^2} \right). \quad (16)
$$

By using the results of [34], the integral I_1 can be written as:

$$
I_1 = \log_2 \left(\frac{1}{(2\pi\sigma^2)^{N_r/2}} \right) - \frac{N_r}{2 \log_e 2}. \quad (17)
$$

By following the Jensen's inequalty-based approach described in [35], [36] and employing (16) in the integral I_2, we can simplify it to obtain:

$$
I_2 \geq -2 \log_2 N_t + \frac{N_r}{2} \log_2 \left(\frac{1}{2\pi\sigma^2} \right) - \frac{N_r}{2}
$$
$$
+ \log_2 \left[\sum_{l,m=1}^{N_t} \exp\left[\sum_{r=1}^{N_r} -\frac{(x_{r,l} - x_{r,m})^2}{4\sigma^2} \right] \right]. \quad (18)
$$

Now, the DCMC capacity of OSSK can be obtained by substituting (17) and (18) in (15), and by following the approximating approach of [36] as:

$$
C_{\text{DCMC}} \approx 2 \log_2 N_t - \log_2 \left[N_t \right.
$$
$$
\left. + \sum_{\substack{l,m=1 \\ m \neq l}}^{N_t} \exp\left[-\frac{\bar{\gamma} \log_2 N_t}{2N_r^2} \sum_{r=1}^{N_r} (h_{r,l} - h_{r,m})^2 \right] \right]. \quad (19)
$$

Remark 2: From (13) and (19), it is palpable that, in order to calculate APEP and the DCMC capacity, we need to find the pdf of difference of two correlated $\Gamma\Gamma$ RVs, i.e., $h_{l_1} - h_{l_2} = z$.

Proposition 1 (PDF of difference of two correlated $\Gamma\Gamma$ RVs): The pdf of difference of two arbitrarily correlated $\Gamma\Gamma$ RVs for $z \geq 0$ is given by:

$$
f_Z(z) = \sum_{i_1=0}^{\infty} \sum_{t_1=0}^{\infty} \sum_{k=0}^{\infty} \left[\left(\frac{w_{1,1}^{(\beta)} \Omega^{(\alpha)}}{w_{1,1}^{(\alpha)} \Omega^{(\beta)}} \right)^{2\Upsilon_1} \left(\frac{w_{1,1}^{(\alpha)} w_{1,1}^{(\beta)}}{\Omega^{(\alpha)} \Omega^{(\beta)}} \right)^{\tau} \right.
$$
$$
\left. \times \frac{(-z)^k}{k!} G_{3,3}^{2,3} \left(1 \left| \begin{array}{c} \mathbf{v}_1 \\ \mathbf{v}_2 \end{array} \right. \right) \varrho_{\alpha\beta} \mid_{(N_t=2)} \right], \quad (20)
$$

where $z = h_1 - h_2$, $\tau = k + 1 - \alpha - i_1 - \beta - t_1$, $\Upsilon_1 = \Upsilon_2 \triangleq ((\alpha + i_1 - \beta - t_1)/2)$, $\mathbf{v}_1 = [0, (k - \alpha - i_1 + 1), (k - \beta - t_1 + 1)]$, and $\mathbf{v}_2 = [(\alpha + i_1 - 1), (\beta + t_1 - 1), k]$. The pdf $f_Z(z)$, for $z < 0$ can also be derived with the help of [37, Eq. (6-55)] by following the similar steps as followed for $z \geq 0$, which will lead to the same expression as (20) but with negated z.

TABLE I: Special cases of (20) and the mapping parameters

Mapping method	Resulting pdf
Scenario 1: $\Omega^{(\beta)} = 1/\beta,\ w_{1,1}^{(\beta)} = 1, w_{1,2}^{(\beta)} = 0, t_1 = 0,$ and $\mid \mathbf{W}^{(\beta)} \mid = 1$	$f_Z(z) = \sum\limits_{i_1,k=0}^{\infty} \left[\left(\dfrac{\beta}{\Omega^{(\alpha)}} \right)^{k+1} \left(\dfrac{1}{w_{1,1}^{(\alpha)}} \right)^{2\alpha+2i_1-k-1} \dfrac{(-z)^k}{k!} \right.$ $\left. \times G_{3,3}^{2,3} \left(1 \left\| \begin{matrix} 0, (k-\alpha-i_1+1), (k-\beta+1) \\ (\alpha+i_1-1), (\beta-1), k \end{matrix} \right. \right) \dfrac{\mid \mathbf{W}^{(\alpha)} \mid^{\alpha}\ w_{1,2}^{(\alpha)}\ \mid^{2i_1}}{i_1!\Gamma(\alpha)\Gamma(\alpha+i_1)(\Gamma(\beta))^2} \right]$
No correlation: $\Omega^{(\alpha)} = 1/\alpha,$ $\Omega^{(\beta)} = 1/\beta,\ w_{1,1}^{(\alpha)}, w_{1,1}^{(\beta)} = 1,$ $w_{1,2}^{(\alpha)}, w_{1,2}^{(\beta)} = 0,\ i_1, t_1 = 0,$ and $\mid \mathbf{W}^{(\alpha)} \mid, \mid \mathbf{W}^{(\beta)} \mid = 1$	$f_Z(z) = \sum\limits_{k=0}^{\infty} \left[\dfrac{(\alpha\beta)^{k+1}}{(\Gamma(\alpha)\Gamma(\beta))^2} \dfrac{(-z)^k}{k!} G_{3,3}^{2,3} \left(1 \left\| \begin{matrix} 0, (k-\alpha+1), (k-\beta+1) \\ (\alpha-1), (\beta-1), k \end{matrix} \right. \right) \right]$

Proof: See Appendix A.

Note that, the pdf proposed in (20) is a generalized pdf where correlation is considered to be arising due to both SLSE. However, special cases of this pdf applicable to Scenario 1 of correlation (correlation among large-scale eddies are dominant) and no correlation can also be derived from (20) by using the mapping technique summarized in Table I.

III. AVERAGE PERFORMANCE EVALUATION

In this section, we will evaluate ABER and the average achievable capacity of the considered OSSK-MIMO system with arbitrary correlation. We will first present the performance analysis of OSSK-MISO and in order to extricate some useful insights about G_c and G_d, we will perform asymptotic analysis. Finally, we will extend the analysis to MIMO.

A. Performance Metrices of OSSK-MISO

From Proposition 1, where pdf $f_Z(z)$ is already given in (20), we can easily find the pdf of the absolute of difference of two correlated $\Gamma\Gamma$ RVs, i.e., $a = \mid z \mid$, by employing the transformation of RVs of $f_A(a) = f_Z(a) + f_Z(-a)$, where $f_Z(a) = f_Z(z) \mid_{(z=a)}$ for $z \geq 0$ and $f_Z(-a) = f_Z(z) \mid_{(z=-a)}$ for $z < 0$. From (20) and the discussion following it, we can reasonably state that, $f_Z(a) = f_Z(-a)$, which leads to $f_A(a) = 2f_Z(a)$, therefore the pdf is given by:

$$f_A(a) = \sum_{i_1,t_1=0}^{\infty} \sum_{k=0}^{\infty} 2 \left[\left(\frac{w_{l_1,l_1}^{(\beta)} \Omega^{(\alpha)}}{w_{l_1,l_1}^{(\alpha)} \Omega^{(\beta)}} \right)^{2\Upsilon_1} \left(\frac{w_{l_1,l_1}^{(\alpha)} w_{l_1,l_1}^{(\beta)}}{\Omega^{(\alpha)}\Omega^{(\beta)}} \right)^{\tau} \right.$$
$$\left. \times \frac{(-a)^k}{k!} G_{3,3}^{2,3} \left(1 \left| \begin{matrix} \mathbf{v}_1 \\ \mathbf{v}_2 \end{matrix} \right. \right) \varrho'_{\alpha\beta} \mid_{(N_t=2)} \right], \quad (21)$$

where $\varrho'_{\alpha\beta} = \varrho_{\alpha\beta}$, except for replacing $w_{n,n+1}^{(\alpha)}$ and $w_{n,n+1}^{(\beta)}$ by $w_{l_1,l_2}^{(\alpha)}$ and $w_{l_1,l_2}^{(\beta)}$, respectively.

1) ABER: Substituting $N_r = 1$ in (13), APEP for MISO can be written as:

$$\text{APEP}(l_1 \rightarrow l_2) = \int_0^{\infty} Q \left(a \sqrt{\frac{\bar{\gamma}\log_2 N_t}{2}} \right) f_A(a) da. \quad (22)$$

Substituting (21) in (22) followed by some rearrangement, simplifications, and algebraic manipulations we obtain the

APEP of OSSK for the considered correlated system in the form of:

$$\text{APEP}(l_1 \rightarrow l_2) = \sum_{i_1,t_1,k=0}^{\infty} \left[\left(\frac{w_{l_1,l_1}^{(\beta)} \Omega^{(\alpha)}}{w_{l_1,l_1}^{(\alpha)} \Omega^{(\beta)}} \right)^{2\Upsilon_1} \left(\frac{w_{l_1,l_1}^{(\alpha)} w_{l_1,l_1}^{(\beta)}}{\Omega^{(\alpha)}\Omega^{(\beta)}} \right)^{\tau} \right.$$
$$\left. \times G_{3,3}^{2,3} \left(1 \left| \begin{matrix} \mathbf{v}_1 \\ \mathbf{v}_2 \end{matrix} \right. \right) \frac{(-1)^k \Gamma((k+2)/2) \varrho'_{\alpha\beta} \mid_{(N_t=2)}}{k!(k+1) \left(\frac{\sqrt{\bar{\gamma}\log_2 N_t}}{2} \right)^{k+1} \sqrt{\pi}} \right]. \quad (23)$$

Let us make the following remarks about the derived APEP expression (23).

- Equation (23) is derived from (22) by using Chernoff bound $Q(x) \leq 1/2 \exp(-x^2/2)$. Nevertheless, a tighter upper bound can be obtained by using $Q(x) \leq 1/12 \exp(-x^2/2) + 1/4 \exp(-2x^2/3)$. Moreover, a lower bound can also be obtained by using $Q(x) \geq 1/2 \exp(-x^2/2 - \sqrt{2/\pi}x)$ [38]. Further, in the next subsection, we will also perform asymptotic performance analysis, which give the ABER bounds for higher SNRs.

- The APEP expression in (23) has been derived for Scenario 2 of correlation. However, we can easily obtain APEP for Scenario 1 by setting $\Omega^{(\beta)} = 1/\beta, w_{l_1,l_1}^{(\beta)} = 1, w_{l_1,l_2}^{(\beta)} = 0, t_j = 0,$ and $\mid \mathbf{W}^{(\beta)} \mid = 1$ in (23) to obtain:

$$\text{APEP}_{\rho^{(\beta)}=0}^{(l_1 \rightarrow l_2)} = \frac{\mid \mathbf{W}^{(\alpha)} \mid^{\alpha}}{\Gamma(\alpha) \left[\Gamma(\beta) \right]^2} \sum_{i_1,k=0}^{\infty} \left[\left[\frac{\mid w_{l_1,l_2}^{(\alpha)} \mid^{2i_1}}{i_1!\Gamma(\alpha+i_1)} \right] \right.$$
$$\times \left(\frac{\beta}{\Omega^{(\alpha)}} \right)^{(k+1)} \frac{(-1)^k}{k!} \left(w_{l_1,l_1}^{(\alpha)} \right)^{1-2\alpha-2i_1+k}$$
$$\left. \times \frac{\Gamma((k+2)/2)}{(k+1) \left(\frac{\sqrt{\bar{\gamma}\log_2 N_t}}{2} \right)^{k+1} \sqrt{\pi}} G_{3,3}^{2,3} \left(1 \left| \begin{matrix} \mathbf{v}'_1 \\ \mathbf{v}'_2 \end{matrix} \right. \right) \right], \quad (24)$$

where $\mathbf{v}'_1 = \left[0, (k-\alpha-i_1+1), (k-\beta+1) \right],$ and $\mathbf{v}'_2 = \left[(\alpha+i_1-1), (\beta-1), k \right].$

- We have derived (23) for the correlated $\Gamma\Gamma$ AT channel, nevertheless it is valid for the uncorrelated scenario as well. By setting $\mid \mathbf{W} \mid = 1, \Omega^{(\alpha)} = 1/\alpha, \Omega^{(\beta)} = 1/\beta, w_{l_1,l_1}^{(\alpha)} = w_{l_1,l_1}^{(\beta)} = 1, w_{l_1,l_2}^{(\alpha)}, w_{l_1,l_2}^{(\beta)} = 0$ and $i_j, t_j = 0,$ in (23), we can obtain the APEP expression for OSSK

over the uncorrelated channel as:

$$
\begin{aligned}
\text{APEP}^{(l_1 \to l_2)}_{\rho^{(\alpha)},\rho^{(\beta)}=0} &= \frac{1}{\Gamma(\alpha)\left[\Gamma(\beta)\right]^2} \sum_{k=0}^{\infty} \left[\left[\frac{1}{\Gamma(\alpha)} \right] \right. \\
&\times \left(\alpha\beta \right)^{(k+1)} \frac{(-1)^k}{k!} \frac{\Gamma((k+2)/2)}{(k+1)\left(\frac{\sqrt{\bar{\gamma}}\log_2 N_t}{2} \right)^{k+1} \sqrt{\pi}} \\
&\left. \times G_{3,3}^{2,3} \left(1 \left| \begin{matrix} 0,(k-\alpha+1),(k-\beta+1) \\ (\alpha-1),(\beta-1),k \end{matrix} \right. \right) \right].
\end{aligned}
\tag{25}
$$

Note, in [39, Eq. (22)] APEP was derived for uncorrelated FSO-SSK MISO with weighted Txs. For unity weights, [39, Eq. (22)] becomes the same as (25), which confirms correctness of the mapping technique and the generalized nature of our derived APEP result in (23).

- The expression (23) is valid for arbitrary correlation. However, in case of constant correlation, where all the apertures are equally spaced and because of that all the non-diagonal elements of the correlation matrices $\mathbf{\Sigma}^{(\alpha)}, \mathbf{\Sigma}^{(\beta)}$ have a constant value, i.e., $\sigma_{i,j}^{(\alpha)}, \sigma_{i,j}^{(\beta)} = \rho$ for $i \neq j$ and the elements of $\mathbf{W}^{(\alpha)}, \mathbf{W}^{(\beta)}$ become independent of the Tx's indices. Therefore, for this case, the derived analytical expression APEP, (23), also become independent of the Tx indices (l_1 and l_2), which allows us to take the Q-function outside the summations of (12), and therefore the paired summation reduces to:

$$
\frac{1}{N_t \log_2(N_t)} \sum_{l_1=1}^{N_t} \sum_{l_2=1}^{N_t} d_H(c_{l_1}, c_{l_2}) = \frac{N_t}{2}.
\tag{26}
$$

Employing (23) and (26) in (12), ABER of OSSK for the $\Gamma\Gamma$ AT channel with constant correlation can be derived in the form of:

$$
\begin{aligned}
\text{ABER} &= \sum_{i_1,t_1,k=0}^{\infty} \frac{N_t}{2} \left[\left(\frac{w_{1,1}^{(\beta)}\Omega^{(\alpha)}}{w_{1,1}^{(\alpha)}\Omega^{(\beta)}} \right)^{2\Upsilon_1} \left(\frac{w_{1,1}^{(\alpha)}w_{1,1}^{(\beta)}}{\Omega^{(\alpha)}\Omega^{(\beta)}} \right)^{\tau} \right. \\
&\left. \times \frac{(-1)^k \Gamma((k+2)/2)\varrho''_{\alpha\beta}\,|_{(N_t=2)}}{k!(k+1)\left(\frac{\sqrt{\bar{\gamma}}\log_2 N_t}{2} \right)^{k+1}\sqrt{\pi}} G_{3,3}^{2,3}\left(1 \left| \begin{matrix} \mathbf{v}_1 \\ \mathbf{v}_2 \end{matrix} \right. \right) \right],
\end{aligned}
\tag{27}
$$

where $\varrho''_{\alpha\beta} = \varrho_{\alpha\beta}$, except for replacing $w_{n,n+1}^{(\alpha)}$ and $w_{n,n+1}^{(\beta)}$ by $w_{1,2}^{(\alpha)}$ and $w_{1,2}^{(\beta)}$, respectively.

- Equation (23) is in power series form, nevertheless, it converge for a small and finite number of summations, see Table II. The convergence results and the truncation error (caused by use of finite terms instead of the infinite series) for (23) are summarized in Table II, which shows that the number of summation terms required for convergence and the truncation error increase with the increasing correlation level. We will also prove convergence of the series in the result section (Section IV) by considering an example of convergence test of (24) for Scenario 1, which was obtained from (23) [1].

---

[1] The convergence of the series and truncation error can also be analytically proved by following the method given in [1], [40]. However, because of the limited space in this paper, we have not included these analytical derivation in this paper.

2) Asymptotic characteristics:

At very high SNR, asymptotic APEP can be characterized by two parameters of the G_c and the G_d. The former specifies the relative horizontal shift of BER against the SNR on a log-log scale; whereas, the latter shows the slope of decay of these plots, at asymptotically high values of SNR. Mathematically we have:

$$
\lim_{\bar{\gamma} \to \infty} \text{APEP}(\bar{\gamma}) \approx (G_c \bar{\gamma})^{-G_d}.
\tag{28}
$$

The asymptotic APEP of the considered $N_t \times 1$ system can be obtained by substituting $k = 0$ in (23), since the term corresponding to the smallest exponent of $\bar{\gamma}$ in the power series dominates APEP. Therefore, we have:

$$
\begin{aligned}
\lim_{\bar{\gamma} \to \infty} \text{APEP}(l_1 \to l_2) &= \sum_{i_1,t_1=0}^{\infty} \left[\left(\frac{w_{l_1,l_1}^{(\beta)}\Omega^{(\alpha)}}{w_{l_1,l_1}^{(\alpha)}\Omega^{(\beta)}} \right)^{\Upsilon_1} \varrho'_{\alpha\beta}|_{(N_t=2)} \right. \\
&\left. \times 2 \left(\frac{w_{l_1,l_1}^{(\alpha)}w_{l_1,l_1}^{(\beta)}}{\Omega^{(\alpha)}\Omega^{(\beta)}} \right)^{\tau|_{(k=0)}} \frac{G_{3,3}^{2,3}\left(1 \left| \begin{matrix} \mathbf{v}_1\,|_{(k=0)} \\ \mathbf{v}_2\,|_{(k=0)} \end{matrix} \right. \right)}{\sqrt{\bar{\gamma}}\log_2 N_t \sqrt{\pi}} \right].
\end{aligned}
\tag{29}
$$

By adopting the same substitutions, which was used to obtain (24), the asymptotic APEP expression for Scenario 1 can be obtained as:

$$
\begin{aligned}
\lim_{\bar{\gamma} \to \infty} \text{APEP}^{(l_1 \to l_2)}_{\rho^{(\beta)}=0} &= \frac{|\mathbf{W}^{(\alpha)}|^{\alpha}}{\Gamma(\alpha)\left[\Gamma(\beta)\right]^2} \sum_{i_1=0}^{\infty} \left[\left[\frac{|w_{l_1,l_2}^{(\alpha)}|^{2i_1}}{i_1!\Gamma(\alpha+i_1)} \right] \right. \\
&\left. \times \frac{2\beta(w_{l_1,l_2}^{(\alpha)})^{1-2\alpha-2i_1} G_{3,3}^{2,3}\left(1 \left| \begin{matrix} \mathbf{v}'_1\,|_{(k=0)} \\ \mathbf{v}'_2\,|_{(k=0)} \end{matrix} \right. \right)}{\Omega^{(\alpha)}\sqrt{\bar{\gamma}}\log_2 N_t \sqrt{\pi}} \right].
\end{aligned}
\tag{30}
$$

Remark 3: Meijer-G function in (30), which indicates complexity in the expression, is independent of average SNR, therefore results in a simple asymptotic BER expression. On comparing (29) and (30) with (28) gives $G_d = 1/2$, which shows that, G_d of correlated OSSK FSO-MISO is independent of correlation and number of Txs and is always equal to 0.5. Moreover, comparing (29) with (28), G_c of OSSK-MISO for Scenario 2 is:

$$
\begin{aligned}
G_c = &\left[\sum_{i_1,t_1=0}^{\infty} \left(\frac{w_{l_1,l_1}^{(\beta)}\Omega^{(\alpha)}}{w_{l_1,l_1}^{(\alpha)}\Omega^{(\beta)}} \right)^{2\Upsilon_1} \left(\frac{w_{l_1,l_1}^{(\alpha)}w_{l_1,l_1}^{(\beta)}}{\Omega^{(\alpha)}\Omega^{(\beta)}} \right)^{\tau|_{(k=0)}} \right. \\
&\left. \times \frac{2 G_{3,3}^{2,3}\left(1 \left| \begin{matrix} \mathbf{v}_1\,|_{(k=0)} \\ \mathbf{v}_2\,|_{(k=0)} \end{matrix} \right. \right)}{\sqrt{\bar{\gamma}}\log_2 N_t \sqrt{\pi}} \varrho'_{\alpha\beta}\,|_{(N_t=2)} \right]^{-2}.
\end{aligned}
\tag{31}
$$

Likewise, G_c for Scenario 1 can also be obtained by comparing (28) and (30).

Remark 4 (Dependence of G_c on ρ): For a given AT parameters, G_c in (31) depends on two parameters of correlation level ρ and N_t. However, for Scenario 1, G_c will depend on ρ_α (as only large-scale eddies are correlated) and N_t. Note that, in (31) the exponent of correlation parameters ($w_{l_1,l_1}^{(\alpha)}$ and $w_{l_1,l_1}^{(\beta)}$) is negative, i.e., with increasing level of correlation, G_c must increase. Fascinating insights can be extracted by observing the dependence of G_c on correlation, by using the parameter–coding gain variance (ΔG_c^v); ΔG_c^v can be evaluated by taking

TABLE II: Upper limits of i_1, t_1, k

	$\alpha = 4, \beta = 1.9$			$\alpha = 2, \beta = 1.4$		
	$1 > \rho > 0.9$	$\rho \leq 0.9$	$\rho = 0$	$1 > \rho > 0.9$	$\rho \leq 0.9$	$\rho = 0$
i_1^u	15	10	6	10	6	4
t_1^u	15	10	6	10	6	4
k^u	1	1	1	1	1	1
Truncation error	2×10^{-4}	9×10^{-5}	1×10^{-6}	1×10^{-4}	1×10^{-5}	2×10^{-6}

the logarithmic of the ratio of G_c at a positive value of ρ to the value of G_c at $\rho = 0$ as given below [41]:

$$\Delta G_c^v = 10 \log_{10} \frac{G_c^{(\rho < 1)}}{G_c^{(\rho = 0)}}, \tag{32}$$

where the positive value of ΔG_c^v is the coding gain advantage, while its negative value represents the loss in G_c.

Observation 1: In Fig. 1a, we have shown ΔG_c^v versus ρ_α and ρ for Scenarios 1 and 2 using (32). The discontinuos line denote the ΔG_c^v v/s ρ plot for Scenario 2 and solid line represent the ΔG_c^v v/s ρ_α plot for Scenario 1. It can be observed from the figure that, Scenario 2 offers higher gain compared to Scenario 1. We will further verify this observation in the result section based on the analytical and simulated BER plots.

3) Achievable DCMC capacity: In (19), let us denote $\sum_{r=1}^{N_r} (h_{r,l} - h_{r,m})^2 = a_{l,m}^2$ by $s_{l,m}$ (note that, for a MISO system $N_r = 1$). In order to obtain the achievable DCMC capacity, we first need to evaluate $\mathbb{E}\left[\exp\left(-\frac{\bar{\gamma} \log_2 N_t}{2N_r^2} s_{l,m}\right)\right]$ using (21) as:

$$\mathbb{E}\left[\exp\left(-\frac{\bar{\gamma} \log_2 N_t}{2N_r^2} s_{l,m}\right)\right] = \sum_{i_1,t_1,k=0}^{\infty} \left[\kappa G_{3,3}^{2,3}\left(1 \left| \begin{array}{c} \mathbf{v}_1 \\ \mathbf{v}_2 \end{array}\right. \right) \right.$$
$$\left. \times \Gamma\left(\frac{k+1}{2}\right)\left(\frac{2N_r^2}{\bar{\gamma} \log_2 N_t}\right)^{(k+1)/2} \right], \tag{33}$$

where, $\kappa = \left(\frac{w_{l_1,l_1}^{(\beta)} \Omega^{(\alpha)}}{w_{l_1,l_1}^{(\alpha)} \Omega^{(\beta)}}\right)^{2\Upsilon_1} \left(\frac{w_{l_1,l_1}^{(\alpha)} w_{l_1,l_1}^{(\beta)}}{\Omega^{(\alpha)} \Omega^{(\beta)}}\right)^{\tau}$
$$\times \frac{(-1)^k \varrho_{\alpha\beta}' |_{N_t=2}}{k!}. \tag{34}$$

By substituting (33) into (19), the achievable DCMC capacity is obtained in the form of:

$$C_{\text{DCMC}} \geq 2\log_2 N_t - \log_2 \left[N_t + \sum_{\substack{l,m=1 \\ m \neq l}}^{N_t} \sum_{i_1,t_1,k=0}^{\infty} \left[\kappa \right.\right.$$
$$\left.\left. \times G_{3,3}^{2,3}\left(1 \left| \begin{array}{c} \mathbf{v}_1 \\ \mathbf{v}_2 \end{array}\right. \right) \Gamma\left(\frac{k+1}{2}\right)\left(\frac{2N_r^2}{\bar{\gamma} \log_2 N_t}\right)^{\frac{(k+1)}{2}} \right]\right]. \tag{35}$$

B. Performance Metrices of $N_t \times N_r$ OSSK-MIMO

1) Approximation of absolute value of difference of two correlated $\Gamma\Gamma$ RVs: To extend the BER results obtained for MISO in previous subsections, we will use the conditional PEP from (13). Note that, the exact BER analysis from this formulation requires pdf of summation of the squared absolute value of difference of two correlated $\Gamma\Gamma$ RVs. To the best of authors knowledge, no closed-form of the required pdf is reported in the literature, which makes the BER analysis of correlated

OSSK-MIMO computationally intractable. Nevertheless, we can significantly simplify our analysis by approximating the pdf.

Proposition 2: The pdf of absolute value of difference of two correlated $\Gamma\Gamma$ RVs in case of Scenario 1 (with solution $\rho_{i,j}^{(\beta)} = 0$) for the plane wave under moderate and strong AT can be approximated by an uncorrelated Gamma distribution with $q = 1$ and $\theta \approx 2$, and the approximation remains valid for any level of correlation with $\rho_{i,j}^{(\alpha)} < 1$.

Proof: See Appendix B.

Proposition 3: The pdf of absolute value of difference of two correlated $\Gamma\Gamma$ RVs in case of Scenario 2 (with solution $\rho_{i,j}^{(\alpha)} = \rho_{i,j}^{(\beta)}$) for the plane wave under moderate AT can be approximated by an uncorrelated Gamma distribution with q and θ; where q is independent of ρ with $q = 1$, whereas θ depends on the correlation level, i.e., $\rho_{i,j}^{(\alpha)}$ and $\rho_{i,j}^{(\beta)}$.

Proof: See Appendix C.

2) BER of $N_t \times N_r$ Correlated MIMO-OSSK: By applying the transformation of RVs to the asymptotic pdf of Gamma distributed RV (46), the asymptotic pdf of γ_r is obtained as:

$$f_{\gamma_r}(\gamma_r) = \frac{1}{2\sqrt{\gamma_r \bar{\gamma}}} f_{A_r}(a_r) \big|_{a_r = \sqrt{\frac{\gamma_r}{\bar{\gamma}}}}$$
$$\approx \frac{1}{2\sqrt{\gamma_r \bar{\gamma}}} f_X(x) \big|_{x = \sqrt{\frac{\gamma_r}{\bar{\gamma}}}} = \frac{1}{2\sqrt{\gamma_r \bar{\gamma}} \Gamma(q) \theta^q}\left(\frac{\gamma_r}{\bar{\gamma}}\right)^{\frac{q-1}{2}}, \tag{36}$$

where $q = 1$ and $\theta \approx 2$. Using the standard definition of MGF and employing the identity [31, Eq. (3.381.4)] to it, we can easily obtain MGF of γ_r in the following form:

$$M_{\gamma_r}(s) = \frac{1}{2\theta \bar{\gamma}^{q/2}} \frac{\Gamma(\frac{q}{2})}{s^{\frac{q}{2}}}. \tag{37}$$

Consider $\sum_{r=1}^{N_r} \gamma_r = \gamma_{sm}$ and uncorrelated Rxs, MGF of γ_{sm} can be obtained as $M_{\gamma_{sm}}(s) = \left(M_{\gamma_r}(s)\right)^{N_r}$. We can derive APEP for MIMO-OSSK using (13), by rewritting it in terms of γ_{sm} and then averaging it over γ_{sm}. Moreover, in the resulting expression we replace Gaussian-Q function by its alternative form of $Q(y) = \frac{1}{\pi}\int_0^{\pi/2} \exp\left(-\frac{y^2}{2\sin^2\theta}\right) d\theta$ and then follow MGF-based approach to write APEP in terms of MGF as follows:
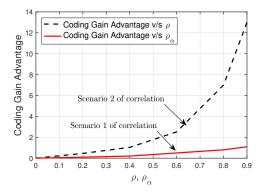
$$\text{APEP}(l_1 \to l_2) = \frac{1}{\pi}\int_0^{\pi/2} M_{\gamma_{sm}}\left(\frac{\log_2 N_t}{4N_r^2 \sin^2\theta}\right) d\theta. \tag{38}$$

Substituting $M_{\gamma_{sm}}(s)$ from (37) in (38) and employing [31, eq. (3.621.3)], the approximate closed-form expression of APEP for MIMO-OSSK with correlation can be obtained as:

$$\text{APEP}(l_1 \to l_2) = \frac{0.5(qN_r - 1)!!}{qN_r!!}$$
$$\times \left[\frac{\Gamma(\frac{q}{2})}{2\theta}\left(\frac{4N_r^2}{\bar{\gamma} \log_2 N_t}\right)^{\frac{q}{2}}\right]^{N_r}. \tag{39}$$

(a) Analytical coding gain advantage vs. correlation of 2 Txs-based MISO-OSSK.

(b) Analytical coding gain loss vs. the number of Txs (N_t) of MIMO-OSSK for $\rho_{i,j}^{(\alpha)} = \rho_{i,j}^{(\beta)} = 0.05$.

Fig. 1: Plots illustrating the variation of coding gain advantage/loss with correlation (ρ, ρ_α and N_t).
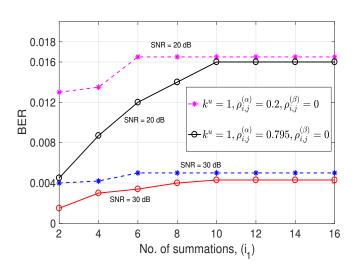

Fig. 2: Convergence test of BER for 2×1 FSO-MISO with Scenario 1 of correlation with $\rho_{i,j}^{(\alpha)} = 0.2, 0.795, \rho_{i,j}^{(\beta)} = 0$ under moderate AT at $\alpha = 4, \beta = 1.9$.

Employing (39) and (26) in (12), the asymptotic BER of MIMO-OSSK can be expressed as:
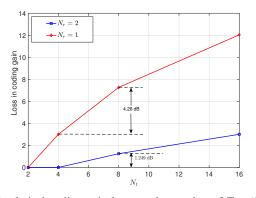
$$\text{ABER} = \frac{N_t}{4} \frac{(qN_r - 1)!!}{qN_r!!} \left[\frac{\Gamma(\frac{q}{2})}{2\theta} \left(\frac{4N_r^2}{\bar{\gamma} \log_2 N_t} \right)^{\frac{q}{2}} \right]^{N_r}. \quad (40)$$

By comparing (40) with (28), we can compute G_d of MIMO-OSSK, which readily gives $G_d = N_r/2$. Therefore, as compared to MISO, in MIMO the G_d of OSSK is increased by the N_r factor. Note, G_c can be expressed as:

$$G_c = \left(\frac{N_t}{4} \frac{(qN_r - 1)!!}{qN_r!!} \left[\frac{\Gamma(\frac{q}{2})}{2\theta} \left(\frac{4N_r^2}{\log_2 N_t} \right)^{\frac{q}{2}} \right]^{N_r} \right)^{\frac{-2}{qN_r}}. \quad (41)$$

It can be observed from (41) that, G_c of OSSK-MIMO depends on q, θ (which changes with the correlation level), N_t, and N_r. Similar to Fig. 1a (where we have shown ΔG_c^v v/s ρ), in Fig. 1b we depict ΔG_c^v vs. N_t using (41) and the relation $\Delta G_c^v = 10 \log_{10} \frac{G_c^{(N_t > 2)}}{G_c^{(N_t = 2)}}$ to observe the loss in G_c incurred in the system for $N_t > 2$ as compared to $N_t = 2$.

Observation 2: It can be observed from Fig. 1b that, for OSSK-MISO with $N_r = 1$, loss in G_c is 4.26 dB at $N_t = 8$ compared to $N_t = 4$. However, for OSSK-MIMO for $N_r = 2$,

improvement in the SE can be achieved at $N_t = 4$ with no SNR penalties as compared to $N_t = 2$, since ΔG_c^v at $N_t = 4$ is zero.

3) Achievable DCMC Capacity of Correlated MIMO-OSSK: We can employ the results of previous subsection and Propositions 2 and 3 to denote $(h_{r,l} - h_{r,m})^2$ by γ_r in (19), where the pdf of γ_r is derived as (36). Now, to derive the achievable capacity from (19), we first need to evaluate $\mathbb{E}\big[\exp\big(-\frac{\bar{\gamma} \log_2 N_t}{2N_r^2} \sum_{r=1}^{N_r} \gamma_r\big)\big]$. By following MGF-based approach and (37) we get:

$$\mathbb{E}\big[\exp\big(-\frac{\bar{\gamma} \log_2 N_t}{2N_r^2} \sum_{r=1}^{N_r} \gamma_r \big) \big] = \prod_{r=1}^{N_r} \left[M_{\gamma_r}\left(\frac{\log_2 N_t}{2N_r^2} \right) \right]$$

$$\approx \prod_{r=1}^{N_r} \left[\frac{\Gamma(q/2)}{2\theta \bar{\gamma}_r^{q/2}} \left(\frac{2N_r^2}{\log_2 N_t} \right)^{q/2} \right]. \quad (42)$$

IV. NUMERICAL RESULTS AND DISCUSSION

In this section, we present a brief discussion of the numerical results obtained using the analytical derivations outlined in Section III and validate the theory using MATLAB simulation. It must be noted that, simulation results are obtained for a correlated $\Gamma\Gamma$ channel with 10^6 samples using the algorithm given in Fig. 4, and Green's matrix approximation of the correlation matrices given in [42]. Moreover, we have calculated values of AT parameters for both plane ($L = 3$ km, $\lambda = 1550$ nm) and spherical waves ($L = 1.5$ km, $\lambda = 850$ nm) under moderate ($\alpha = 4, \beta = 1.9$ and $\alpha = 2.35, \beta = 1.9$, respectively) and strong AT ($\alpha = 4.2, \beta = 1.4$ and $\alpha = 2, \beta = 1.4$, respectively), using the equation for α and β given in [43]. In Fig. 2, we show the BER obtained from (24) as a function of SNR by varying the upper limits of i_1 and k in (24) to demonstrate the convergence of the power series. For SNR ≥ 30 dB, it can be seen from the figure that the BER plots converge after $i_1 = t_1 = 10, k = 1$ in case of moderate AT with $\alpha = 4, \beta = 1.9, N_t = 2$, and $\rho = 0.795$. However, for strong AT ($\alpha = 2$ and $\beta = 1.4$) the series converges early at $i_1 = t_1 = 6, k = 1$.

Figure 3 demonstrates the analytical and simulated BER performance as a function of the average SNR for OSSK-based FSO-MISO with 2 Txs for both uncorrelated ($\rho \approx 0$) and correlated ($\rho = 0.2, 0.77, 0.886, 0.92, 0.956$) channels under
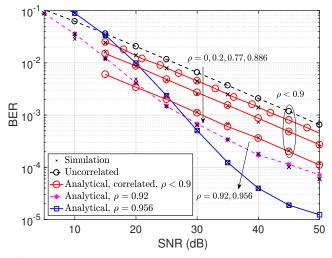
Fig. 3: Analytical and simulated BER vs. the average SNR of OSSK for 2×1 FSO-MISO at different ρ.

moderate AT with $\alpha = 4, \beta = 1.9, \Omega^{(\alpha)} = \Omega^{(\beta)} = 1$ [21]. It must be pointed out that, the analytical results for $\rho \approx 0.2$ (Scenario 1: $\rho_{i,j}^{(\alpha)} = 0.795, \rho_{i,j}^{(\beta)} = 0$) and the plots for $\rho = 0.77, 0.786, 0.886$ (corresponding to Scenario 2) are obtained using (24) and (23), respectively. The analytical plots corresponding to the correlation of $\rho > 0.9$ are obtained using the ensemble average of (13). Note the following important observations: (i) there is a good match between the simulation and predicted results for all the considered cases, thus validating the correctness of analysis; (ii) the BER plots for $\rho = 0.2$ (Scenario 1: $\rho_{i,j}^{(\alpha)} = 0.795, \rho_{i,j}^{(\beta)} = 0$) offer a G_c of $\approx 2.5-3$ dB over the uncorrelated case; and (iii) for Scenario 2 $(\rho_{i,j}^{(\alpha)} = \rho_{i,j}^{(\beta)})$ with $0.9 > \rho > 0.2$, the BER performance is improved at higher correlation levels by providing G_c up to 15 dB. For the plane wave under moderate AT, a G_c of approximately 13 dB is achieved at $\rho = 0.886$ compared with $\rho \approx 0.2$. Note, a higher level of G_c of 8.2 dB is achieved as ρ is merely increased from 0.77 to 0.886. However, as the correlation increases beyond $\rho > 0.9$, a crossover is observed with the plots of lower correlation value. It means that, the OSSK performs poorer for $\rho > 0.9$ at the lower SNR range of 0-25 dB as compared with the system with $\rho < 0.9$. However, at higher SNR values (i.e., > 25 dB), it can still provide a significant G_c of 3-17 dB over the system with $\rho < 0.9$. The intuitive and logical explanation for this unanticipated result can be given as follows.

Remark 5 (**Reason for the improved performance at high ρ and crossover at $\rho > 0.9$**): In the case of OSSK for the correlated system, rather than a single channel with several sub-channels, the effective channel is actually the difference of two sub-channels, i.e., $h_{l_1} - h_{l_2}$, and the BER performance depends on the statistics of the effective channel. If we calculate the variance of $h_{l_1} - h_{l_2}$ at different correlation levels, it will be observed that, the value of variance reduces with the increasing value of correlation level, thus making the effective channel more deterministic at higher value of correlation[2]. Furthermore, at high correlation, fading fluctuations of each of

the effective channel change jointly. These conditions jointly lead to improved BER performance at very high correlation levels for Scenario 2. A similar observation of an improvement in BER performance at higher correlation level was also reported in [7, Fig. 5], which was applicable to a MISO-RF system. However, at $\rho > 0.9$ and for the lower SNR range (0-25 dB) differentiating between different channels become a challenging task at the Rx, thus resulting in poor performance. At SNR > 25 dB, we notice a significant G_c over the lower correlation levels.

Observation 3: Under moderate AT, OSSK-MISO employed to correlated FSO with Scenario 2 of correlation ($\rho_{i,j}^{(\alpha)} = \rho_{i,j}^{(\beta)}$), offers substantial increase in G_c by 13 dB at a BER of 10^{-3} with $\rho = 0.886$ compared with $\rho \approx 0.2$ for $N_t = 2$.

Figure 5 compares the BER performance of the considered system under moderate ($\alpha = 4, \beta = 1.9$) and strong AT ($\alpha = 2, \beta = 1.4$) with $N_t = 4, 8$, for a range of correlation models of constant, circular, and linearly arbitrary correlation matrices proposed in [42] and the calculated AT parameters (mentioned at the beginning of this section). It should be noted that, $\rho_{const}^{(\alpha)}$, $\rho_{circ}^{(\alpha)}$, and $\rho_{arbit}^{(\alpha)}$ in the figure denote the correlation coefficients between the large-scale eddies of the first and the ith Tx (for $i = 2, 3, 4$) corresponding to constant, circular, and arbitrary correlation models, respectively. We have obtained the BER of OSSK for 4×1 FSO from (12) and (24) using BER $= \frac{1}{4}(P(1 \rightarrow 2) + 2P(2 \rightarrow 3) + P(3 \rightarrow 4) + P(2 \rightarrow 4) + P(1 \rightarrow 3) + 2P(1 \rightarrow 4))$ by considering correlation between every two links. Following are the important observations to be noted: (i) for the considered correlation levels/models, the linearly arbitrary correlation model offers a marginal coding gain of 1.5-2 dB over the other two correlation models in case of moderate AT; however, in case of strong AT, the BER plots corresponding to all the correlation models almost overlap with each other; and (ii) there is an improvement in the BER performance with the reduced number of Txs. At a BER of 2×10^{-4}, the SNR penalties are 3.5 and 6 dB for moderate and strong AT, respectively, as N_t is increased from 4 to 8, thus the trade-off between the SE and the BER performance.

Figure 6 depicts Monte Carlo simulations ($\circ$ marker) and predicted (solid lines) BER against the SNR for $N_t = 2$ and $N_r = 1, 2, 3, 4$, and under moderate AT and low correlation (i.e., $\rho \approx 0.2$), obtained from the correlated MIMO-OSSK model (Scenario 1) proposed in Subsection III-B. At asymptotically high values of SNR (> 20 dB), there is a good agreement between analytical and simulation results, which verifies the correctness of the proposed analytical model, and also validates the accuracy of the approximation propsed as Proposition 2. In addition, the BER performance is unchanged for $\rho_{i,j}^{(\alpha)} < 1, \rho_{i,j}^{(\beta)} = 0$ (as was observed in Fig. 3 for MISO) regardless of AT. We also observe that, the BER sharply improve with N_r for SNR > 15 dB. Note that, all BER plots except for $N_r = 1$ are below the forward error correction (FEC) BER limit of 3.8×10^{-3}. Further, G_d of the system from BER plots is obtained by taking the logarithm of the ratio of two BER values at the SNR values with a step of 10 dB for different values of ρ and N_t. E.g., in case of MIMO with $N_r = 2$, the BER values are 7.17×10^{-5} and 6.4×10^{-4}

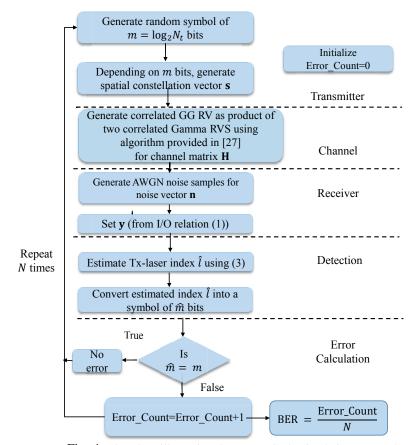[2]We have not given the numerical data to support this observation because of lack of space.

Fig. 4: Flowchart illustrating the Monte Carlo simulation approach.

Fig. 5: Analytical and simulated BER vs. the average SNR of OSSK for 2×1 FSO-MISO at different ρ.
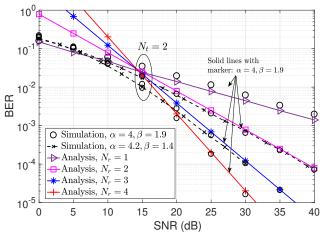

Fig. 6: Comparison between Monte Carlo simulation and analytical BER versus the average SNR of MIMO-OSSK for $N_t = 2$ and for strong and moderate AT at a correlation level of $\rho_{i,j}^{(\alpha)} = 0.795$, $\rho_{i,j}^{(\beta)} = 0$ ($\rho \approx 0.2$).

at the SNR values of 40 and 30 dB, respectively from Fig. 6, which gives $G_d = 0.95 \approx N_r/2 = 1$. Similar sets of calculations are repeated for $N_r = 1, 3, 4$ and it is observed that $G_d = N_r/2$.

Figure 7 compares the predicted BER results of correlated MIMO-OSSK (Scenario 1) under moderate AT ($\alpha = 4, \beta = 1.9$) for a range of N_t and $N_r = 1, 2, 3$. Having established in Figs. 3-5 that, the correlation in Scenario 1 with $\rho_{i,j}^{(\beta)} = 0$

does not significantly affect the BER performance of OSSK and therefore, we have obtained the BER plots for Scenario 1 at a fixed correlation of $\rho_{i,j}^{(\alpha)} = 0.795, \rho_\beta = 0$. Detailed study of the figure shows that, (i) the BER improves with N_r as expected; and (ii) at a BER of 10^{-3} (i.e., below the FEC limit) and for $N_r = 1$, the SNR penalities are 2.6 and 7 dB for N_t of 4 and 8 compared to N_t of 2. However, for $N_r = 3$,
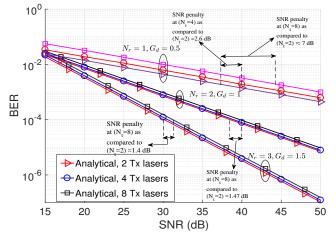
Fig. 7: Moderate AT ($\alpha = 4, \beta = 1.9$) for $N_t = 2, 4, 8$, and $N_r = 1, 2, 3$ for Scenario 1 of correlation.
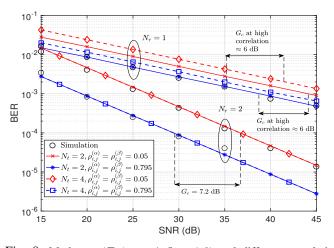

Fig. 8: Moderate AT ($\alpha = 4, \beta = 1.9$) and different correlation levels for $N_t = 2, 4$, and $N_r = 1$ and 2 for Scenario 2 of correlation.

the SNR penalties significantly reduces to 0.4 and 1.4 dB.

In Fig. 8, we compare the predicted analytical and simulated BER plots of MIMO-OSSK with correlation for Scenario 2 where both large-and small-scale eddies equally contribute to the effective correlation level under moderate AT ($\alpha = 4, \beta = 1.9$). Contrary to the Figs. 6-7 (where no significant effect of correlation on the BER performance was noticed), in Fig. 8, very interesting and surprising results are noticed when the BER at low correlation ($\rho = 0.043$) is compared with that at a high ($\rho = 0.77$) correlation level. The existence of a correlated channel (which in general is supposed to degrade the system's performance) has been turned to the considered system's advantage with $N_t = 2, 4$, as G_c of 6 and 7.2 dB are observed for N_r of 1 and 2, respectively, at higher levels of correlation.

Observation 4: Similar to MISO, in MIMO also an improved SE is achieved at the cost of increased SNR penalties. However, for MIMO, the amount of SNR penalty is substantially reduced and also G_d is improved with N_r. Note that, in case of MIMO-OSSK (i.e., $N_r = 2$), the BER plots of $N_t = 2$ and $N_t = 4$ overlap, which means that without incurring any SNR penalty, a higher SE of 2 bits/s/Hz can be achieved with $N_t = 4$ as compared to 1 bit/s/Hz with $N_t = 2$. (*Note that, this*
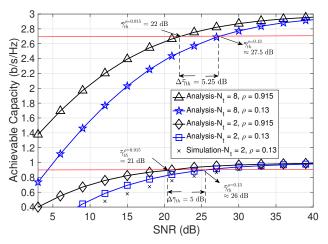

Fig. 9: Achievable DCMC capacity versus the average SNR plots of MISO-OSSK system under moderate AT ($\alpha = 4, \beta = 1.9$) for $N_t = 2, 8$ with $\rho = 0.13$ and 0.915.
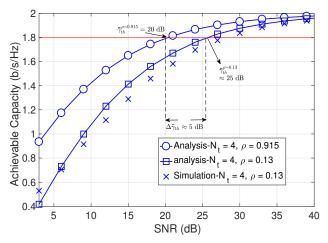

Fig. 10: Achievable DCMC capacity versus the average SNR plots of MISO-OSSK system under moderate AT ($\alpha = 4, \beta = 1.9$) for $N_t = 4$ and $\rho = 0.13$ and 0.915.

observation is in agreement with Observation 2). Moreover, a G_c of 7.2 dB can be achieved at $\rho = 0.77$ compared with $\rho = 0.05$. The explanation of this unpredictable result is same as that of Fig. 3 for MISO.

Having established that, the correlated AT channel offers improved error performance for OSSK, let us analyse the impact of correlation on the achievable DCMC capacity of OSSK [3]. In Figs. 9 and 10, we compare the achievable capacity of OSSK-MISO for two different correlation levels of $\rho = 0.13$ (low) and $\rho = 0.915$ (high), $\alpha = 4$, $\beta = 1.9$, and different values of N_t. We also compare the analytical results with the plots obtained through simulation (ensemble average of (19)). It is evident from the figure that, the simulation results closely follow the analytical plots, thus validating the analysis presented in Section III-A. The term $\bar{\gamma}_{th}$ used in the figure denotes the threshold level for the SNR at which 90% of the maximum achievable capacity (C_{max}) is attained, whereas $\Delta \bar{\gamma}_{th}$ shows the change in the two $\bar{\gamma}_{th}$ observed at

---

[3]Unless otherwise stated, the DCMC plots considering correlation of $\rho \leq 0.25$ corresponds to scenario 1 of correlation while the results with $\rho > 0.25$ corresponds to the scenario 2 of correlation.

This article has been accepted for publication in a future issue of this journal, but has not been fully edited. Content may change prior to final publication. Citation information: DOI 10.1109/TWC.2019.2955449, IEEE Transactions on Wireless Communications
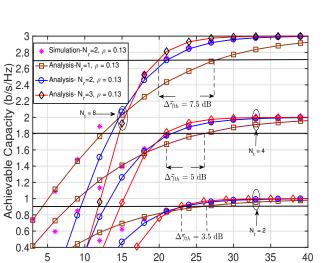
12

Fig. 11: Comparison of analytical and simulated achievable capacity versus the average SNR plots of MIMO-OSSK for $N_t = 2, 4, 8$, $N_r = 1, 2, 3$, and $\rho = 0.13$.
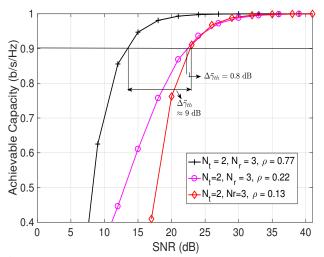

Fig. 12: Achievable DCMC capacity versus the average SNR plots of MIMO-OSSK with 1bit/s/Hz under moderate AT ($\alpha = 4$, $\beta = 1.9$) and for $\rho = 0.13, 0.22$ and 0.77.

two different correlation levels, i.e., $\Delta\bar{\gamma}_{th} = \bar{\gamma}_{th}^{\rho_1} - \bar{\gamma}_{th}^{\rho_2}$. Note that, for all the three cases considered with the SE of 1, 2, and 3 bits/s/Hz, $\Delta\bar{\gamma}_{th} \approx 5$ dB. Moreover, the capacity of OSSK improves at higher value of correlation, since the value of $\bar{\gamma}_{th}$ reduces with the increasing value of ρ, i.e., when $\rho_1 < \rho_2$ then $\bar{\gamma}_{th}^{\rho_1} > \bar{\gamma}_{th}^{\rho_2}$.

Figure 11 compares the simulated results with the predicted asymptotic achievable capacity ((42)) of MIMO-OSSK for different values of N_r and the spectral efficiencies of 1, 2, and 3 bits/s/Hz. Note that, all plots are obtained for $\rho = 0.13$ by employing the approximate pdf proposed in *Proposition 2*. A good matching between the analysis and simulation is observed within the useful range of SNR. As expected, the SE improves with the increasing value of N_r, i.e., $\bar{\gamma}_{th}^{N_{r_2}} < \bar{\gamma}_{th}^{N_{r_1}}$ if $N_{r_2} > N_{r_1}$. Moreover, the difference in two threshold SNRs ($\Delta\bar{\gamma}_{th}$) observed at two different values of N_r increases with the increasing value of N_t. For instance, $\Delta\bar{\gamma}_{th} = 3.5$ dB for $N_t = 2$, however, for $N_t = 4$ it increases to 5 dB and further increases to 7.5 dB for $N_t = 8$.
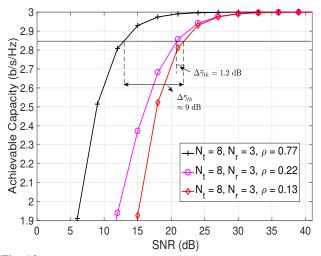

Fig. 13: Achievable DCMC capacity versus the average SNR plots of MIMO-OSSK with 3 bits/s/Hz under moderate AT ($\alpha = 4, \beta = 1.9$) and for $\rho = 0.13, 0.22$ and 0.77.

In Figs. 12 and 13, the achievable capacity of the OSSK-MIMO ($N_r = 3$) is compared for ρ of 0.13, 0.22, and 0.77 and for N_t of 2 and 8, repectively. Similar to MISO, the achievable capacity of MIMO-OSSK significantly improves with the higher correlation levels. Note, (i) $\bar{\gamma}_{th}$ is 23 dB for $\rho = 0.13$ and reduces to 14 dB for $\rho = 0.77$, which results in improved system performance in terms of the achievable capacity with $\Delta\bar{\gamma}_{th} = 9$ dB; (ii) $\Delta\bar{\gamma}_{th}$ values are nearly same for $N_t = 2$ and 8 and a similar trend was observed in MISO-OSSK as well; and (iii) the improvement achieved in the DCMC capacity at higher correlation levels is substantially more for MIMO-OSSK.

V. EXPERIMENTAL INVESTIGATION

In this section, we introduce the experimental setup developed for a correlated FSO system [4] followed by the performance evaluation of the correlated links.

1) Experimental Setup: The laboratory experimental setup for the correlated FSO system is composed of two Tx apertures (Tx_1, Tx_2), a FSO channel with a link length (L) of 3 m, and a Rx (see Fig. 14). Since in SSK, only one Tx is active at a time, both Txs are connected to a signal source (i.e., BER tester - BERT-VeEX VEPAL TX300) via a fiber optic switch (Thorlabs OSW-1310E). The laser outputs from both Txs are launched into the free space channel via two gradient-index (GRIN) fiber optic collimators (Thorlabs 50-1550A-APC). Two plano convex lenses (aperture of 2.54 cm) with focal lengths of 10 cm and 15 cm, respectively, are used to minimize the beam divergence. At the Rx, a plano convex lens of $f = 15$ cm and a GRIN fiber collimator are used to couple the incoming optical beam onto single mode fibers (SMF). The output of SMF, which is attenuated using a digital variable attenuator in order to adjust the level of optical SNR, is amplified using the erbium-doped fiber amplifier (EDFA). The amplifier output is applied to the optical spectrum analyzer

---

[4]The experimental setup was developed at Czech Technical University in Prague.
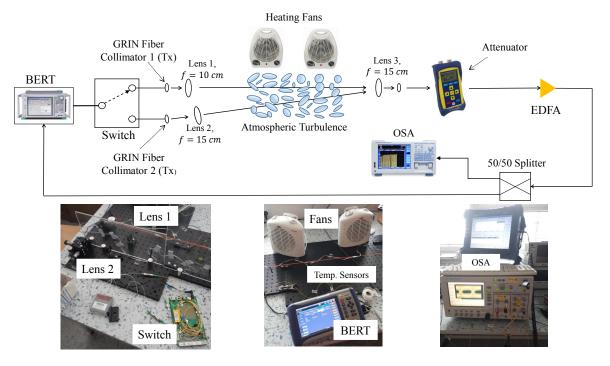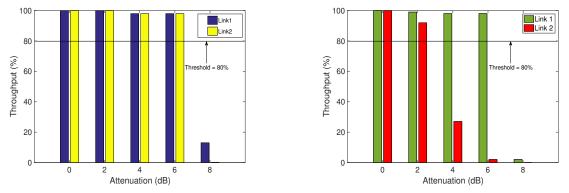
Fig. 14: Block diagram and snapshot of experimental setup of the correlated FSO system.

(a) Comparison of throughput vs. the attenuation for FSO links with $C_n^2 = 2.116 \times 10^{-14} \mathrm{m}^{-2/3}$ (same AT in both the links) at $\rho = 0.98$ (Case A).

(b) Comparison of throughput vs. attenuation for FSO links 1 and 2 with $C_n^2 = 6.569 \times 10^{-10} \mathrm{m}^{-2/3}$ and $1.67 \times 10^{-10} \mathrm{m}^{-2/3}$, respectively, at $\rho \approx 0$ (Case B).

Fig. 15: Experimental results for the throughput against the attenuation for FSO links 1 and 2.
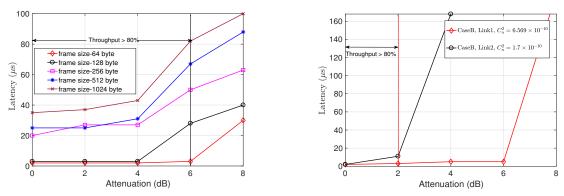
(OSA) and BERT for measurement and the characterization of the proposed system. The correlated links' throughput and latency with and without turbulance at low and high correlation levels are measured using BERT. Note that, we have used an controlled indoor AT chamber to create turbulence by blowing hot air using two fans. The strength of turbulence is varied by controlling the speed/heating level of fans. 20 temperature sensors each placed 0.225 m apart between the Tx and the Rx are used to record the temperature profile along the FSO path, which are used to calculate C_n^2 by using the equation given in [23].

2) Experimental Results: It is well known that, the channel capacity is a theoretical term and practically the throughput of the system, which gives the lower limit of the capacity, can be measured. Therefore, we have recorded the measured throughput and latency for a 3m FSO link by considering two different scenarios. Case A - The Txs are placed 6 cm aparts and we measured C_n^2 of $2.116 \times 10^{-14} \mathrm{m}^{-2/3}$ and σ_R^2 of 0.778 common for links. These parameters were used to determine AT parameters using (4) and (5) of $\alpha = 4.8, \beta = 3$. Further, using (6) we calculated ρ to be 0.98. Case B - Both fans were on, blowing hot air into the particular channels which were partly separated near Tx end (by 1.12 m) and part of link was common, thus this setup resulted to an uncorrelated FSO system with $C_n^2 = 6.569 \times 10^{-10} \mathrm{m}^{-2/3}, \sigma_R^2 = 0.309$ in Link 1 and $C_n^2 = 1.67 \times 10^{-10} \mathrm{m}^{-2/3}, \sigma_R^2 = 0.078$ in Link 2.

From Fig. 15a it can be observed that, the throughputs are the same for both links under AT and high correlation of 0.98 level. Moreover, the required threshold OSNR to achieve a threshold throughput of 80% for both links at an attenuation of 6 dB is 35 dB and the links become unreliable for the

(a) Latency recorded during experiment at different attenuation levels for the setup with $C_n^2 = 2.116 \times 10^{-14} \mathrm{m}^{-2/3}$ (same AT in both links) at $\rho = 0.98$ (Case A).

(b) Latency recorded during experiment at different attenuation levels in both FSO links 1 and 2 with $C_n^2 = 6.569 \times 10^{-10} \mathrm{m}^{-2/3}$ and $1.67 \times 10^{-10} \mathrm{m}^{-2/3}$, respectively, at $\rho \approx 0$ (Case B).

Fig. 16: Experimental results for the latency against the attenuation for FSO links 1 and 2.

attenuation ≥ 8 dB [5]. Figure 15b corresponds to Case B with a very low correlation level ($\rho \approx 0$) and unbalanced AT links (measured AT levels in both links are not similar and the turbulence is comparatively higher than the previous case). In this case, the performances of both links are not comparable and therefore, $\bar{\gamma}_{th}^{op} = \max(\bar{\gamma}_{th}^{op1}, \bar{\gamma}_{th}^{op2}) = 37.5$ dB, which is higher than $\bar{\gamma}_{th}^{op} = 35$ dB for the correlated setup, where $\bar{\gamma}_{th}^{op1}$ and $\bar{\gamma}_{th}^{op2}$ are the threshold OSNR for links 1 and 2, respectively. Note that, the link with a higher AT level (Link 1) offers an improved performance in terms of the throughput than the other link with a comparatively lower AT level.

Remark 6: The required threshold value of OSNR to achieve the throughput of 80% for the correlated setup is 2.5 dB lower than the uncorrelated setup, i.e., the system with correlation performs better in terms of the throughput. Note that, this observation is in agreement with the analytical findings for the DCMC capacity shown in Fig. 9, where the required threshold SNR to achieve a threshold capacity of 90% reduces with the increasing correlation level.

In Figs. 16a and 16b, we have measured the latency (in μs) for both setups under different attenuation levels. Figure 16a exhibits the latency measured for Case A when both links are balanced (i.e., same AT) and highly correlated. In order to study the impact of symbol (or bit) duration on the latency and throughput of the considered system, we have taken the readings by changing the frame size from 64 byte to 1024 byte. It can be observed that, the latency increases with frame size, however, it does not affect the throughput [6]. In Fig. 16b, we illustrate the latency measured for Case B with two uncorrelated unbalanced links. Since the Tx$_2$ was kept at a small angle to maintain a LOS path with the Rx, the measured latency of link 2 is greater than that of link 1.

VI. CONCLUSIONS

We have conducted the BER and the achievable capacity performance analysis of the OSSK-based FSO-MIMO system
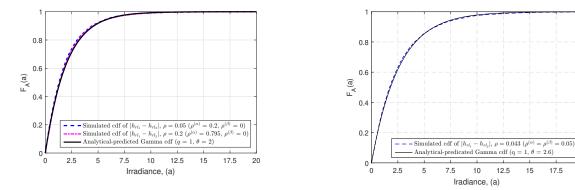
over an arbitrarily correlated $\Gamma\Gamma$ turbulence channel. A correlated channel is in general likely to degrade the system's performance, nonetheless, we have shown that the use of OSSK in a correlated FSO system leads to an unanticipated and interesting observation of significant improvement in the BER performance in terms of SNR by 13 dB at a high correlation level of $\rho = 0.886$ compared to $\rho \approx 0.2$ for $N_t = 2, N_r = 1$. Improvement in BER performance with increasing correlation level can be obtained upto the correlation value of $\rho \leq 0.9$. In addition, we outlined that, the G_d of OSSK depends only on the number of receiving apertures. Moreover, a substantial improvement in the capacity of OSSK-MISO is achieved at higher correlation levels, as compared with low correlation levels. Further, from the experimental investigation, an improvement in the performance of the system in terms of throughput has been observed in the system with higher correlation levels and lower AT levels as compared to the system with lower correlation and higher AT levels.

APPENDIX A
PROOF OF PROPOSITION 1

By employing some mathematical simplification to the earlier derived pdf (10) for $N_t = 2$, we can obtain the joint pdf $f_{H_1,H_2}(h_1,h_2)$ in the following form:

$$f_{H_1,H_2}(z+h_2,h_2) = \sum_{i_1,t_1=0}^{\infty} \left[\left(\frac{w_{1,1}^{(\beta)}\Omega^{(\alpha)}}{w_{1,1}^{(\alpha)}\Omega^{(\beta)}} \right)^{\Upsilon_1} \left(\frac{w_{2,2}^{(\beta)}\Omega^{(\alpha)}}{w_{2,2}^{(\alpha)}\Omega^{(\beta)}} \right)^{\Upsilon_2} \right.$$
$$\times \left(\frac{w_{1,1}^{(\alpha)}w_{1,1}^{(\beta)}}{\Omega^{(\alpha)}\Omega^{(\beta)}} \right)^{-\mu_1+1} G_{0,2}^{2,0}\left(\frac{w_{2,2}^{(\alpha)}w_{2,2}^{(\beta)}h_2}{\Omega^{(\alpha)}\Omega^{(\beta)}} \Big| \begin{matrix} \cdot,\cdot \\ \mathbf{v} \end{matrix} \right) \varrho_{\alpha\beta}\mid_{N_t=2}$$
$$\left. \times \left(\frac{w_{2,2}^{(\alpha)}w_{2,2}^{(\beta)}}{\Omega^{(\alpha)}\Omega^{(\beta)}} \right)^{-\mu_2+1} G_{0,2}^{2,0}\left(\frac{w_{1,1}^{(\alpha)}w_{1,1}^{(\beta)}(z+h_2)}{\Omega^{(\alpha)}\Omega^{(\beta)}} \Big| \begin{matrix} \cdot,\cdot \\ \mathbf{v} \end{matrix} \right) \right], \quad (43)$$

where $\mathbf{v} = \left[(\alpha+i_1-1),(\beta+t_1-1) \right]$, $\mu_1 = \mu_2 \triangleq ((\alpha+i_1+\beta+t_1)/2)$ and $\Upsilon_1 = \Upsilon_2 \triangleq ((\alpha+i_1-\beta-t_1)/2)$. Substituting (43) in [37, Eq. (6-55)] for $z \geq 0$, followed by some algebraic

---

[5]Note, at an attenuation of 0 and 8 dB, the measured OSNR in links 1 and 2 of Case A were 41 dB and 33 dB, and for Case B were 39.5 dB and 31.5 dB.

[6]Since both the links are balanced and highly correlated in this case, latencies measured in both the links are same.

(a) Cdfs of absolute value of difference of two correlated $\Gamma\Gamma$ RVs for Scenario 1 ($\rho_{i,j}^{(\alpha)} = 0.795, 0.2$) and its predicted approximation as uncorrelated Gamma RV ($q = 1$, $\theta = 2$) for moderate AT $\alpha = 4, \beta = 1.9$.

(b) Cdfs of absolute value of difference of two correlated $\Gamma\Gamma$ RVs for Scenario 2 ($\rho_{i,j}^{(\alpha)} = \rho_{i,j}^{(\alpha)} = 0.05$) and its predicted approximation as uncorrelated Gamma RV ($q = 1$, $\theta = 2.6$) for moderate AT $\alpha = 4, \beta = 1.9$.

Fig. 17: Comparison of simulated cdfs of absolute of diffrence of two correlated $\Gamma\Gamma$ and its predicted approximations for Scenarios 1 and 2 at different values of correlation.

manipulations [7], we have:

$$
f_Z(z) = \sum_{i_1, t_1 = 0}^{\infty} T_{corr} \left[\int_0^{\infty} G_{0,2}^{2,0} \left(\frac{w_{1,1}^{(\alpha)} w_{1,1}^{(\beta)} z}{\Omega^{(\alpha)} \Omega^{(\beta)}} + t \left| \begin{matrix} \cdot, \cdot \\ \mathbf{v} \end{matrix} \right. \right) \right.
$$
$$
\left. \times G_{0,2}^{2,0} \left(t \left| \begin{matrix} \cdot, \cdot \\ \mathbf{v} \end{matrix} \right. \right) \left(\frac{w_{1,1}^{(\alpha)} w_{1,1}^{(\beta)}}{\Omega^{(\alpha)} \Omega^{(\beta)}} \right)^{-1} \varrho_{\alpha\beta} \left|_{N_t=2} \, dt \right], \tag{44}
$$

where $T_{corr} = \left(\frac{w_{1,1}^{(\beta)} \Omega^{(\alpha)}}{w_{1,1}^{(\alpha)} \Omega^{(\beta)}} \right)^{2\Upsilon_1} \left(\frac{w_{1,1}^{(\alpha)} w_{1,1}^{(\beta)}}{\Omega^{(\alpha)} \Omega^{(\beta)}} \right)^{-2\mu_1 + 2}$. Using [44, Eq. (2.24.1.3)] in (44), we can derive the pdf (20) of difference of two arbitrarily correlated $\Gamma\Gamma$ RVs.

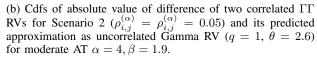## APPENDIX B
PROOF OF PROPOSITION 2

In PEP formulation (13), let us denote the absolute value of difference of two correlated $\Gamma\Gamma$ RVs at rth Rx, $| h_{rl_1} - h_{rl_2} |$, by another RV a_r, i.e., $a_r = | h_{rl_1} - h_{rl_2} | = | z |$ and $\gamma_r = a_r^2 \bar{\gamma}$. We can obtain the asymptotic pdf of a_r for Scenario 1 from (21) by considering the series in the equation near origin at $k = 0$ and employing the same transformation method for (24) to procure:

$$
f_{A_r}(a_r) = \sum_{i_1 = 0}^{\infty} \frac{2 \mid \mathbf{W}^{(\alpha)} \mid^{\alpha}}{\Gamma(\alpha) [\Gamma(\beta)]^2} (w_{l_1, l_1}^{(\alpha)})^{1 - 2\alpha - 2i_1} \left(\frac{\beta}{\Omega^{(\alpha)}} \right)
$$
$$
\times \left[\frac{\mid w_{l_1, l_2}^{(\alpha)} \mid^{2i_1}}{i_1! \Gamma(\alpha + i_1)} \right] G_{3,3}^{2,3} \left(1 \left| \begin{matrix} 0, (1 - \alpha - i_1), (1 - \beta) \\ (\alpha + i_1 - 1), (\beta - 1), 0 \end{matrix} \right. \right). \tag{45}
$$

Let x be another RV following Gammma distribution with the asymptotic pdf near origin given as:

$$
f_X(x) = \frac{1}{\Gamma(q) \theta^q} x^{q-1}. \tag{46}
$$

where q and θ are the shape-and scale-parameters, respectively, with $q, \theta > 0$. In order to approximate the pdf of a_r by another known statstical model, we first compare the exponents of RVs a_r and x in (45) and (46), respectively. It can be easily observed from the comparison that we can describe the

behavior of A_r using the Gamma pdf only if $q = 1$. Having obtained one parameter, further we employ the curve fitting technique using MATLAB to obtain the best fit parameter θ for a given set of AT parameters and correlation level.

Remark 7: From curve fitting we find that, for $\rho_{i,j}^{(\alpha)} < 1, \rho_{i,j}^{(\beta)} = 0$ and under moderate ($\alpha = 4, \beta = 1.9$) and strong AT ($\alpha = 4.2, \beta = 1.4$), the value of θ remains unaltered, i.e., $\theta \approx 2$ in all the cases of Scenario 1.

APPENDIX C
PROOF OF PROPOSITION 3

Considering (21) near origin at $k = 0$, the asymptotic pdf of a_R for Scenario 2 can be obtained as:

$$
f_{A_r}(a_r) = \sum_{i_1, t_1 = 0}^{\infty} 2 \left(\frac{w_{l_1, l_1}^{(\alpha)} w_{l_1, l_1}^{(\beta)}}{\Omega^{(\alpha)} \Omega^{(\beta)}} \right)^{\tau|_{k=0}} \left(\frac{w_{l_1, l_1}^{(\beta)} \Omega^{(\alpha)}}{w_{l_1, l_1}^{(\alpha)} \Omega^{(\beta)}} \right)^{2\Upsilon_1}
$$
$$
\times G_{3,3}^{2,3} \left(1 \left| \begin{matrix} 0, (1 - \alpha - i_1), (1 - \beta - t_1) \\ (\alpha + i_1 - 1), (\beta + t_1 - 1), 0 \end{matrix} \right. \right) \varrho_{\alpha\beta}' \left|_{(N_t=2)} \right. . \tag{47}
$$

By comparing the exponents of x in (46) and a_r in (47), we can easily obtain one parameter, i.e., $q = 1$. Nonetheless, the best fit values of θ for different correlation levels can be evaluated with the help of curve fitting technique using MATLAB. For instance, under moderate AT at $\rho = 0.043$ and 0.77, the absolute value of difference of two correlated $\Gamma\Gamma$ RVs, $| h_{rl_1} - h_{rl_2} |$, can be approximated by an uncorrelated gamma RV with $q = 1, \theta = 2.6$ and $q = 1, \theta = 6$, respectively.

We have validated the correctness of Propositions 2 and 3 in Figs. 17a and 17b by comparing the analytical cummulative distribution function (cdf) of the proposed approximation with the cdf of A_r obtained through MATLAB simulation by considering the moderate AT at $\rho_{i,j}^{(\alpha)} = 0.2, 0.795, \rho_{i,j}^{(\beta)} = 0$ in Fig. 17a and $\rho_{i,j}^{(\alpha)} = \rho_{i,j}^{(\beta)} = 0.043$ in Fig.17b.

In Fig. 17a, the plot with discontinuous line represents the simulated cdf of $| h_{rl1} - h_{rl2} |$ with $\rho_{i,j}^{(\alpha)} = 0.2$, dash-dot line denote the simulated cdf of $| h_{rl1} - h_{rl2} |$ with $\rho_{i,j}^{(\alpha)} = 0.795$, and the solid line represents the analytical result of the proposed approximation as Gamma cdf with $q = 1, \theta = 2$. It is evident from Fig. 17a that, all the three plots very closely follow each other, thus validating the correctness of

our proposed approximation. Likewise, in Fig. 17b the dashed blue line represents the simulated cdf of $\mid h_{rn1} - h_{rn2} \mid$ with $\rho_{i,j}^{(\alpha)} = \rho_{i,j}^{(\beta)} = 0.043$ and the black solid line represents the analytical result of the proposed approximation as Gamma cdf with $q = 1, \theta = 2.6$. A very good match between the simulated and the approximate analytical results can be observed from Fig. 17b, which substantiates the approximation proposed for Scenario 2 of correlation in Proposition 3.

Remark 8: Similarly, we can compare the simulated cdf of $\mid h_{rl1} - h_{rl2} \mid$ for Scenario 1 under strong AT (with $\alpha = 4.2, \beta = 1.4$, and $\rho_{i,j}^{(\alpha)} < 1, \rho_{i,j}^{(\beta)} = 0$) with the predicted analytical gamma cdf ($q = 1, \theta \approx 2$) and a good match will be observed between them.

Remark 9: In case of Scenario 2 of correlation, at a correlation level of $\rho = 0.77$ ($\rho_{i,j}^{(\alpha)} = \rho_{i,j}^{(\beta)} = 0.795$), $\mid h_{rl_1} - h_{rl_2} \mid$ can be approximated by an uncorrelated gamma distribution with $q = 1, \theta = 6$, which can also be validated by obtaining similar cdf plots as obtained in Fig. 17b.

It concludes our proof that, Gamma pdf $f_X(x)$ with $q = 1, \theta \approx 2$ can be used as an approximate pdf of $f_{A_r}(a_r)$ for Scenario I. Moreover, q remains unchanged for Scenario 2, however, θ increases with ρ.

REFERENCES

[1] R. Priyadarshani, A. Jaiswal, M. R. Bhatnagar, Z. Ghassemlooy, and S. Zvanovec, "Performance of space shift keying over a correlated gamma-gamma FSO-MISO channel," *Proc. 11th International Symp. on Commun. Sys., Netw. and Digit. Signal Process. (CSNDSP), Budapest, Hungary,* Jul. 2018.

[2] Y. A. Chau and S. H. Yu, "Space modulation on wireless fading channels," *IEEE Veh. Technol. Conf.,* vol. 3, pp. 1668–1671, Oct. 2001.

[3] R. Y. Mesleh, H. Haas, S. Sinanovic, C. W. Ahn, and S. Yun, "Spatial modulation," *IEEE Trans. Veh. Technol.,* vol. 57, no. 4, pp. 2228–2241, July 2008.

[4] A. Alshamali and B. Quza, "Performance of spatial modulation in correlated and uncorrelated Nakagami fading channel," *J. Commun.,* vol. 4, no. 3, pp. 170–174, Apr. 2009.

[5] R. Mesleh, H. Elgala, and H. Haas, "Optical spatial modulation," *J. Opt. Commun. Netw.,* vol. 3, no. 3, pp. 234–244, Mar. 2011.

[6] J. Jeganathan, A. Ghrayeb, L. Szczecinskiand, and A. Ceron, "Space shift keying modulation for MIMO channels," *IEEE Trans. Wiereless Commun.,* vol. 8, no. 7, pp. 3692–3703, 2009.

[7] M. D. Renzo and H. Haas, "A general framework for performance analysis of space shift keying (SSK) modulation for MISO correlated Nakagami-m fading channels," *IEEE Trans. Commun.,* vol. 58, no. 9, pp. 2590–2603, Sept. 2010.

[8] ——, "Space shift keying (SSK-) MIMO over correlated Rician fading channels: performance analysis and a new method for transmit-diversity," *IEEE Trans. Commun.,* vol. 59, no. 1, pp. 116–129, Jan. 2011.

[9] M. Abazaa, R. Mesleha, A. Mansourb, and M. Aggoune, "The performance of space shift keying for free-space optical communications over turbulent channels," *Proc. SPIE,* vol. 9387, 2015.

[10] R. Mesleh, R. Mehmood, H. Elgala, and H. Haas, "Indoor MIMO optical wireless communication using spatial modulation," in *Proc. IEEE International Conference on Communication (ICC),* Cape Town, South Africa, May 2010, pp. 1–5.

[11] W. O. Popoola, E. Poves, and H. Haas, "Spatial pulse position modulation for optical communications," *IEEE/OSA J. Lightw. Technol.,* vol. 30, no. 18, pp. 2948–2954, July 2012.

[12] T. Ozbilgin and M. Koca, "Optical spatial modulation over atmospheric turbulence channels," *IEEE/OSA J. Lightw. Technol.,* vol. 33, no. 11, pp. 2313–2323, Jun. 2015.

[13] K. P. Peppas and P. T. Mathiopoulos, "Free-space optical communication with spatial modulation and coherent detection over H-K atmospheric turbulence channels," *IEEE J. Lightwave Technol.,* vol. 33, no. 20, pp. 4221–4232, Aug. 2015.

[14] T. Fath, H. Haas, M. Di Renzo, and R. Mesleh, "Spatial modulation applied to optical wireless communications in indoor LOS environments," in *Proc. IEEE Global Telecommunications Conference (GLOBECOM),* Houston, USA, Dec. 2011, pp. 1–5.

[15] M. K. Simon and M. S. Alouni, *Digital Communication over Fading Channels,* 2nd ed. New York, NY: John Wiley & Sons Inc., 2004.

[16] T. Fath and H. Haas, "Performance comparison of MIMO techniques for optical wireless communications in indoor environments," *IEEE Trans. Commun.,* vol. 61, no. 2, pp. 733 – 742, Mar. 2012.

[17] R. Mesleh, H. Elgala, and H. Haas, "Optical spatial modulation," *IEEE/OSA J. Opt. Commun. Netw.,* vol. 3, no. 3, pp. 234–244, Mar. 2011.

[18] W. O. Popoola, S. Sinanovic, and H. E. Nistazakis, "Enhancing the error performance of optical ssk under correlated channel condition," in *IEEE International Conference on Communications Workshops (ICC),* Kuala Lumpur, Jul. 2016.

[19] M. D. Renzo and H. Haas, "On the performance of space shift keying MIMO systems over correlated rician fading channels," in *International ITG Workshop on Smart Antennas (WSA),* Bremen, Apr. 2010, pp. 72–79.

[20] ——, "Performance comparison of different spatial modulation schemes in correlated fading channels," in *IEEE International Conference on Communications,* Cape Town, Jul. 2010.

[21] Z. Ghassemlooy, W. Popoola, and S. Rajbhandari, *Optical Wireless Communications: System and Channel Modelling with MATLAB.* CRC Press, Inc. Boca Raton, FL, USA, 2012.

[22] H. Kaushal and G. Kaddoum, "Optical communication in space: Challenges and mitigation techniques," *IEEE Comm. Surv. Tut.,* vol. 19, no. 1, pp. 57–96, Aug. 2017.

[23] L. C. Andrews and R. L. Phillips, *Laser Beam Propagation through Random Media,* Second ed. SPIE PRESS BOOK, 2005.

[24] D. S. Shiu, G. J. Foschini, M. J. Gans, and J. M. Kahn, "Fading correlation and its effect on the capacity of multielement antenna system," *IEEE Trans. on Commun.,* vol. 48, no. 3, pp. 502–513, Mar. 2000.

[25] G. Arfken, *Mathematical Methods for Physicists,* 3rd ed. Orlando, FL: Academic Press, 1985.

[26] J. Zhang, M. Matthaiou, G. K. Karagiannidis, and L. Dai, "On the multivariate gamma-gamma distribution with arbitrary correlation and applications in wireless communications," *IEEE Trans. Veh. Technol.,* vol. 65, no. 5, pp. 3834–3840, May 2016.

[27] Z. Song, K. Zhang, and Y.L. Guan, "Generating correlated Nakagami fading signals with arbitrary correlation and fading parameters," *IEEE Int. Conf. Comm. (ICC),* vol. 3, pp. 1363–1367, 2002.

[28] G. K. Karagiannidis, D. A. Zogas, and S. A. Kotsopoulos, "An efficient approach to multivariate Nakagami-m distribution using Green's matrix approximation," *IEEE Trans. Commun.,* vol. 2, no. 5, pp. 883–889, Sept. 2003.

[29] M. M. Abadi, Z. Ghassemlooy, S. Zvanovec, M. R. Bhatnagar, M. A. Khalighi, and Y. Wu, "Impact of link parameters and channel correlation on the performance of FSO systems with the differential signaling technique," *IEEE J. Opt. Commun. Netw.,* vol. 9, no. 2, pp. 138–148, Feb. 2017.

[30] G. Yang, M. A. Khalighi, Z. Ghassemlooy, and S. Bourennane, "Performance evaluation of receive-diversity free-space optical communications over the correlated gamma-gamma fading channels," *Appl. Opt.,* vol. 52, no. 24, Aug. 2013.

[31] I. S. Gradshteyn and I. M. Ryzhik, *Table of Integrals, Series, and Products,* 7th ed., Alan Jeffrey, Ed. New York, NY, USA: Academic, 2007.

[32] T.V. Pham, T.C. Thang, and A.T. Pham, "On the ergodic capacity of MIMO correlated gamma-gamma fading channels," in *Proc. of International Conf. on Advanced Technol. for Commun. (ATC),* Oct. 2016.

[33] L. Hanzo, O. Alamri, M. El-Hajjar, and N. Wu, *Near-Capacity MultiFunctional MIMO Systems: Sphere-Packing, Iterative Detection and Cooperation.* New York, NY, USA: Wiley and IEEE Press, 2009.

[34] P.E. Mcillree, "Channel capacity calculations for M-ary N-dimensional signals sets," *Thesis,* The university of South Australia School of Electronics Engineering, Feb. 1995.

[35] C. Bockelmann, D. Wubben, and K. D. Kammeyer, "Mutual information based rate adaptation for MIMO-OFDM systems with finite signal alphabets," *Proc. International ITG Workshop on Smart Antennas (WSA),* pp. 60–67, Feb. 2008.

[36] S. Guo, H. Zhang, J. Zhang, and D. Yuan, "On the mutual information and constellation design criterion of spatial modulation MIMO systems,"

This article has been accepted for publication in a future issue of this journal, but has not been fully edited. Content may change prior to final publication. Citation information: DOI 10.1109/TWC.2019.2955449, IEEE Transactions on Wireless Communications

17

in *Proc. IEEE International Conference on Communication Systems (ICCS), Macau, China*, Nov. 2014.

[37] A. Papoullis and S. U. Pillai, *Probability, Random Variables and Stochastic Processes*, 4th ed.   Tata McGraw-Hill, 2008.

[38] A. Mastin and P. Jaillet, "Log-quadratic bounds for the Gaussian Q-function," Available: https://arxiv.org/abs/1304.2488, Apr. 2013.

[39] A. Jaiswal, M. R. Bhatnagar, and V. K. Jain, "Performance evaluation of space shift keying in free-space optical communication," *IEEE J. Opt. Commun. Netw.*, vol. 9, no. 2, pp. 149–160, Feb. 2017.

[40] M. R. Bhatnagar, "A one bit feedback based beamforming scheme for FSO MISO system over gamma-gamma fading," *IEEE Trans. Commun.*, vol. 63, no. 4, pp. 1306–1318, Apr. 2015.

[41] R. Priyadarshani, M. R. Bhatnagar, Z. Ghassemlooy, and S. Zvanovec, "Effect of correlation on BER performance of the FSO-MISO system with repetition coding over gamma-gamma turbulence," *IEEE Photon. J.*, vol. 9, no. 5, pp. 1–15, Aug. 2017.

[42] ——, "Outage analysis of a SIMO FSO system over an arbitrarily correlated $\mathcal{M}$-distributed channel," *IEEE Photon. Technol. Lett.*, vol. 30, no. 2, pp. 141–144, Jan. 2018.

[43] O. M. Hasan, "Bit error rate and outage rate results for non-zero turbulence cells over gamma-gamma free-space optical wireless channel," *J. Opt. commun.*, vol. 34, pp. 385–391, Dec. 2013.

[44] A. P. Prudnikov, Yu Brychkov, and O. I. Marichev, *Integral and Series, Part 3: More Special Functions*, G. G. Gould, Ed.   Nauka Publishers, 1990, vol. 3.